Hochschule Flensburg

B A C H E L O R – T H E S I S

Thema: Functional validation of meningioma 1 gene

von: Clara Wiebensohn

Matrikel-Nr.: 650778

Studiengang: Biotechnologie, Lebensmitteltechnologie und Verfahrenstechnik

Betreuer/in und
Erstbewerter/in: Prof. Dr. Holger Rehmann

Zweitbewerter/in: Dr. Marketa Kaucka Petersen

Ausgabedatum: 08.02.2022

Abgabedatum: 07.04.2022

Functional validation of meningioma 1 gene

Bachelor thesis

as part of the degree program

Biotechnologie, Lebensmitteltechnologie und Verfahrenstechnik

Flensburg University of Applied Sciences

and

Max Planck Institute for Evolutionary Biology

Submitted by Clara Wiebensohn

Student ID: 650778

April 2022

First referee: Prof. Dr. Holger Rehmann

Second referee: Dr. Marketa Kaucka Petersen

MAX-PLANCK-INSTITUT FÜR EVOLUTIONSBIOLOGIE

Hochschule Flensburg University of Applied Sciences

Table of Contents

List of Abbreviations

α-MEM	α-Minimum Essential Medium
AP	Alkaline phosphatase
ARS	Alizarin Red S
BCIP/ NBT	5-bromo-4-chloro-3-indolyl-phosphate/nitro blue tetrazolium
CPC	Cetylpyridinium chloride
CRISPR	Clustered regularly interspaced short palindromic repeats
DMEM	Dulbecco's Modified Eagle's Medium
DNA	Deoxyribonucleic acid
dNTP	Deoxynucleotid triphosphate
DPBS	Dulbecco's phosphate-buffered saline
FBS	Fetal bovine serum
FACS	Fluorescence-activated cell sorting
FW	Forward
GFP	Green fluorescent protein
HCR	Hybridisation chain reaction
HDR	Homology-directed repair
KO	Knock-out
Mn1	*meningioma 1*
MN1	*MN1* (*MN1* proto-oncogene, transcriptional regulator)
µl	microliter
mM	millimole
mqH_2O	MilliQ water
NHEJ	Non-homologous end joining
PCR	Polymerase chain reaction
Pen Strep	Penicillin-streptomycin
PFA	Paraformaldehyde
pH	*pondus hydrogenii* = potential of hydrogen
RNA	Ribonucleic acid
RV	Reverse

Abstract

The most complex part of the vertebrate body is the head. This intricate structure forms during early embryonic development. However, it remains unclear which genetic and developmental mechanisms underlie the wide variability in head formation and shaping. Many studies have identified genes that play a fundamental role in head development. One of the genes with a prominent function in skull formation is the de-novo evolved meningioma 1 (*Mn1*). Genome editing tools such as CRISPR/Cas9 offer excellent opportunities to study gene function. Herein, the aim was to establish a mutant cell line from the murine osteogenic cells MC3T3-E1. Therefore, CRISPR/Cas9 methodology was employed to generate perturbations in the *Mn1* gene. Whether such genetic perturbation was successful has yet to be validated. Additionally, to carry out the functional validation of the disrupted *Mn1* gene in the mutant cell line, the *in vitro* model of osteoblast differentiation was optimised, together with a battery of staining procedures to assess the levels of alkaline phosphatase and Calcium during this process. The staining procedures were optimised using the original unperturbed MC3T3-E1. The results show that the cells can differentiate into osteoblasts, and the staining methods BCIP/NBT and Alizarin Red S reliably detect the differentiation hallmarks. Furthermore, the differentiation capacity of these cells depends on their age (~passage), which must be taken into consideration for future experiments.

1. Introduction

The vertebrate head is an excellent example of the highly evolvable nature of complex traits. This intricate structure comprises several types of tissues and cells assembled and integrated together during early embryonic development [1]. Studies identified several essential molecules affecting the head's integrity and geometry, and cellular dynamics during head morphogenesis were outlined [1,2]. However, a complex understanding of the genetic and molecular networks controlling head formation and shaping is still missing [2]. It is still largely obscure which genetic and developmental mechanisms underlie the wide variability in phenotypes of vertebrates and how their morphology evolves to attain their distinctive three-dimensional final shape [3,4].

Recent studies focused on identifying the genetic factors underlying morphological differences to address some of the remaining questions. These investigations are also driven by a solid medical interest, as disturbances of developmental signalling and mechanisms at any stage of early embryogenesis result in a broad spectrum of craniofacial abnormalities. Such malformations and asymmetries significantly impact the survival and quality of life and can occur in form of mild facial anomalies and asymmetries, cleft lip and palate or severe conditions influencing feeding, breathing, and neonatal survival. These so-called craniofacial syndromes account for around 30% of all congenital anomalies in humans [1,5]. Some of the syndromes were linked to specific gene(s) mutations and raised the general interest in identifying their processes and functions.

One of the genes with a prominent evident function in skull formation is the *meningioma 1* (*Mn1*) gene in *Mus musculus* (house mouse) and its orthologous gene in humans, the *MN1* (*MN1* proto-oncogene, transcriptional regulator) [6,7]. A proportion of recent reports on patients suffering from the cleft palate or other craniofacial disorders connect these abnormalities with microdeletions in the *MN1* locus [8,9].

Initially, the *Mn1* gene was known for its association with cancer, specifically with a meningioma – a tumor occurring in membranes of the brain [10]. The first cloning and characterisation suggested that *Mn1* acts as a tumor suppressor gene. Balanced translocation of *Mn1* results in its inactivation and contributes to the pathogenesis of meningioma [10]. In addition, the fusion gene TEL/*MN1* is associated with acute myeloid leukaemia – a neoplastic

disease of the hematopoietic system [11]. The following analysis revealed that the MN1 protein is rich in proline residues, contains two regions of polyglutamine stretches, and may act as a transcriptional cofactor [12].

Subsequent investigations using an *Mn1* mutant mouse model revealed that *Mn1* significantly affects skull formation and shaping. The *Mn1* Knock-out (KO) mouse model lacks exon 1 of the *Mn1* gene and manifests severe defects in the head formation. Specifically, intermembranous bones of the skull are either absent or severely disrupted. These defects result in embryonic lethality or death shortly after birth [13]. Studies using calvarial osteoblasts (the cells that drive cranial bone formation) derived from *Mn1* KO mice revealed an essential role of *Mn1* in osteoblast proliferation, differentiation, and function [14].

Genome-wide association studies (GWAS) revealed that *Mn1* significantly affects shape variation and is pleiotropic. Analysis of evolutionary origin showed that this gene arose at the base of bony vertebrates, with the first evidence of an ossified skull. *Mn1* is evidently an essential gene in cranial development and skull shape determination [15].

However, the specific functional role of *Mn1* in evolution and development remains unclear. Further investigations of its function in bone development mechanisms, such as the differentiation and physiology of calvarial osteoblasts, are of great interest. Therefore, to investigate *Mn1* function in the development of the cranial bones and MN1-associated signalling, the osteoblastic cell line MC3T3-E1 derived from newborn mice's calvaria was selected.

This work aimed to establish mutation cell lines of the MC3T3-E1 with targeted perturbation(s) in the *Mn1* gene. For this purpose, custom-designed gene editing constructs were introduced into the cells by transfections. The transfected cells were sorted to allow the single cells to form a clone. The mutant clones were grown till they reached a sufficient cell number to take samples for DNA extraction and analysis by genotyping. Parallel to this project, differentiation, and two staining assays were tested on different passages of the unmodified MC3T3-E1 cells. In the future, the differentiation capacity and transcriptome of the expanded mutated clones will be compared with the original MC3T3-E1 subclone to validate the function of the *Mn1* gene.

2. Theoretical Background

2.1. Mn1

Mn1 in *mus musculus* (house mouse) is located on chromosome 5 and spans about 40 kb. The gene consists of at least two exons of about 4.5 kb and 2.4 kb, with a protein-coding sequence of around 3.8 kb (see Figure 1) [6,16].

Figure 1: structure of *meningioma 1* (*Mn1*)

2.2. MC3T3-E1

The MC3T3-E1 cells are adherent murine precursor osteoblasts. These cells have mesenchymal-like properties and serve as common progenitors for osteoblasts, adipocytes, and chondrocytes in developing skeletal tissues [14]. MC3T3-E1 has multiple derivative clones widely used in bone tissue engineering research. Since their establishment in 1981, studies using MC3T3 cells have been cited over 4000 times [17–19]. In 1999, a series of subclones derived from the original MC3T3-E1 were established. The clones were divided into two groups for further characterisation: "mineralising" and "non-mineralising". The characterisation was based on several criteria, including the expression levels of specific osteoblast genes, the presence of the differentiation markers, and the ability to mineralise [19,20].

For this project, the MC3T3-E1 "mineralising" subclone 4 was used which was bought from the commercial culture collection of *Public Health England*. This subclone from the MC3T3-E1 established in 1981 is phenotypically heterogeneous to the primary osteoblast and was selected for its high potential for osteogenesis [21]. Figure 2 shows a picture of these cells at a confluence of 70%. The cells exhibit a fibroblast-like morphology.

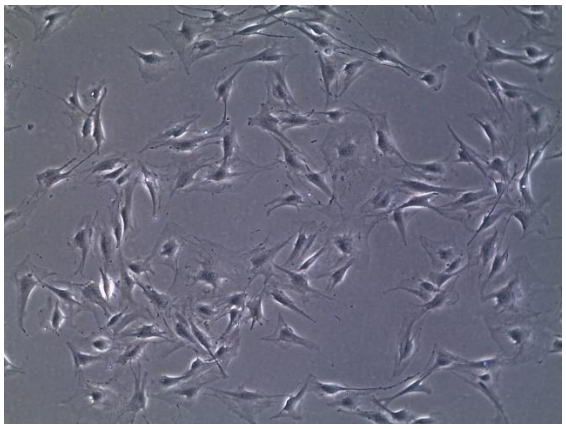

Figure 2: phase-contrast image MC3T3-E1 subclone 4 cells at ~70 % confluence

In preparation for this project, an *in situ* hybridisation chain reaction (HCR) was performed on the MC3T3-E1 to validate that the cell line is expressing *Mn1* (see Figure 3). The HCR is an isothermal enzyme-free nucleotide polymerisation method to visualise specific nucleotides in diverse organisms by using metastable fluorescent hairpins [22]. This method was chosen because it allows direct localisation of the single mRNAs in the cells. The co-staining with DAPI allows visualisation of the nuclei for a better orientation. It confirmed that the cells highly express the *Mn1* gene, making them a perfect *in vitro* model system to investigate the effect of *Mn1* on cell differentiation ability.

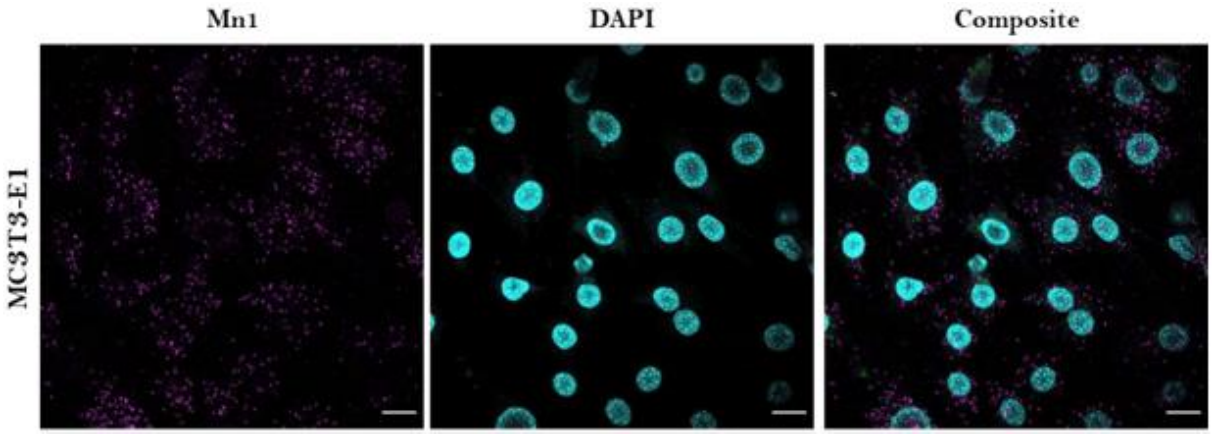

Figure 3: Mn1 in situ hybridisation in MC3T3-E1 (by Elio Escamilla Vega)

2.3. Targeted genome-editing of eukaryotic cells

With genome editing methods, it is possible to make targeted changes in the genes of various organisms. Several genome-editing methods have been developed in recent years. For the targeted modification of the *Mn1* gene in the MC3T3-E1 cells, the experimental setup presented in Figure 4 was designed. As a gene modification tool, the CRISPR/*Cas9* gene-editing system was selected and delivered to the cells in the form of a plasmid. The CRISPR/Cas9 plasmid was introduced into the cells via lipid-based transfection (lipofection). The construct contained the sequence coding as well for a fluorescent protein (GFP, green fluorescent protein), which enabled identifying the successfully transfected cells. The cells were subsequently sorted based on the fluorescence into wells as single cells. Each of the single cells grew to form a clone. When the cells expanded enough, part of each clone was collected and used for DNA isolation. Each of the samples was genotyped by PCR amplification of a specific locus and assessed by agarose-gel-electrophoresis.

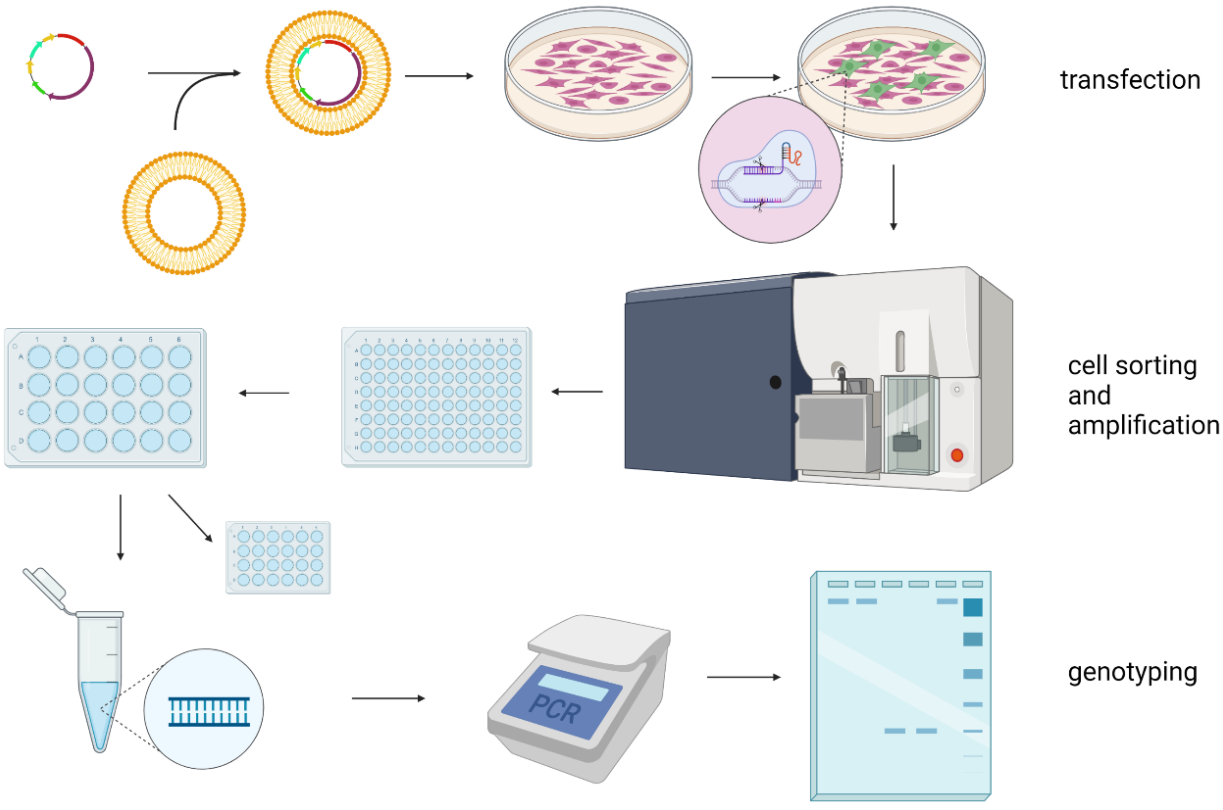

Figure 4: experimental setup for targeted genome-editing of *Mn1* in the MC3T3-E1 cell line and the expansion of individual clones (Created with BioRender.com)

2.3.1. CRISPR/Cas9

The CRISPR/Cas9 is an efficient tool for the targeted DNA cutting and modification of DNA. The clustered regularly interspaced short palindromic repeats (CRISPR), CRISPR-associated protein 9 (Cas9) system was initially known as bacteria and archaea defence mechanism. It protects them against invading viruses by using the endonuclease *Cas*. This restriction enzyme cuts double-stranded DNA at specific sites recognised by guide RNAs [23]. The *Cas9*-enzyme is derived from the bacterium *S. pyogenes*. Engineered versions of the CRISPR/Cas9-system can be used to modify genomes of eukaryotic cells [24].

CRISPR/Cas9-systems are commercially available from different providers in the form of plasmids. The functionality of such an editing tool requires the co-expression of two components: the DNA cutting *Cas9* endonuclease and the engineered single-guide RNA (sgRNA). The sgRNA binds to *Cas9* and recognises a specific sequence of the DNA. As soon as the CRISPR/Cas9 enters the nucleus, the DNA is screened until finding a so-called PAM-sequence - a short DNA sequence usually 2-6 bp (for *Cas9,* it is 5'-NGG-'3), which allows the *Cas9* to unwind the double helix. Only when the PAM-sequence is found, and simultaneously the sgRNA is complementary to the DNA sequence, the cut of double-stranded DNA is carried out [24,25].

The DNA double-strand break generated by the CRISPR system directly activates the cell's repair mechanisms. These include non-homologous end joining (NHEJ) and homology-directed repair (HDR). The most predominant is NHEJ, which occurs at all cell cycle stages and is often considered a "quick-fix" method. It is based on the mechanism of re-joining blunt ends of DNA with minor processing. NHEJ repairs may result in repairs that resemble the wild-type sequence; nevertheless, this repair is error-prone and often results in an insertion or deletions of one to multiple base pairs. These modifications are referred to as indels and can cause frameshift mutations. Mispositioned stop codon or nonsense transcripts subsequently lead to the resulting protein's absence or modified extent or structure. HDR is the second most common repair mechanism in eukaryotes. It relies on a homologous repair template, such as a sister chromatid, to repair disruptions in the DNA, often resulting in complete gene restoration without indel formation [26].

To modify the MC3T3-E1 cells, the pSp*Cas9*(BB)-2A-GFP (PX458) plasmid was used (purchased from *Addgene*). This plasmid (Figure 5) expresses the *S. pyogenes Cas9* enzyme and has a

backbone suitable for introducing specific sgRNAs. Additionally, the construct contains the sequence coding for the fluorescent 2A-EGFP Protein, a fluorescent marker that can be used for selecting these cells by fluorescence. After the plasmid has been delivered to cells, the fluorescent protein will be expressed [27].

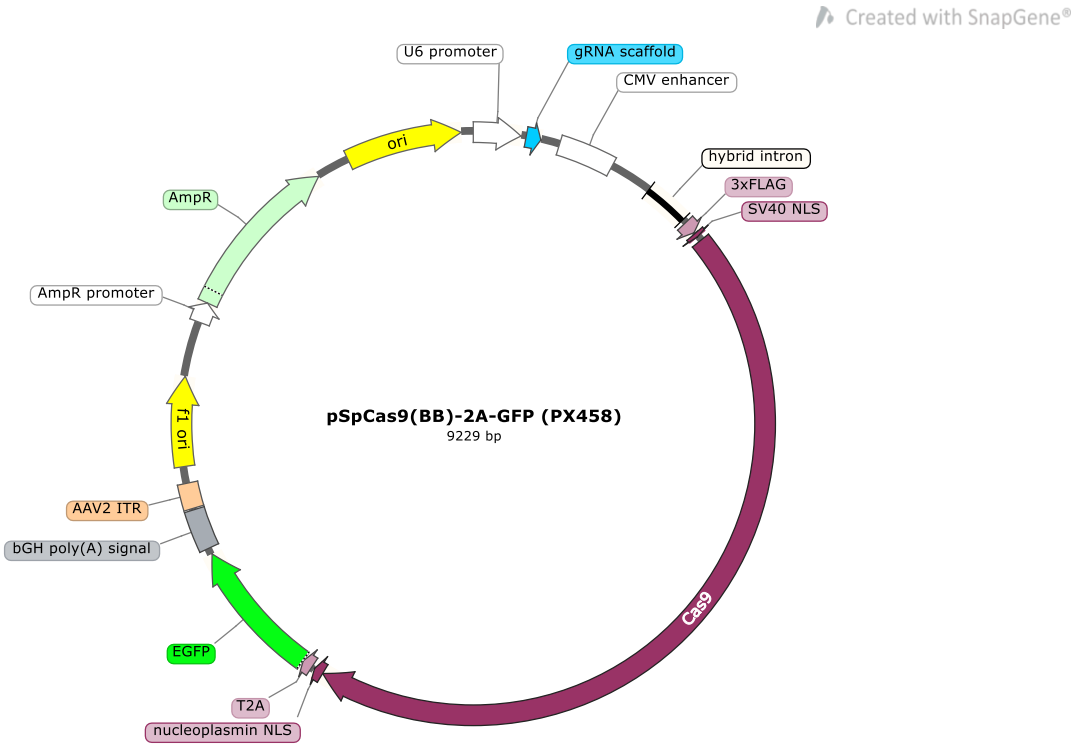

Figure 5: sequence of the pSpCas9(BB)-2A-GFP (PX458) plasmid (https://www.addgene.org/48138/)

In advance of this project, three plasmids were prepared (see Table 1) and

i) sgRNA1, ii) sgRNA2 or iii) both sgRNAs (dgRNA) were cloned into the backbone.

Table 1: description of the guide RNAs for CRISPR/*Cas9* plasmid constructs

plasmid	**target-sequence**
sgRNA1	5'CACCGAGGGGAACTTTAACGAAGCCGG'3
sgRNA2	5'CACCGAACTCAGCCCTTTCACTTCTGG'3
dgRNA	5'CACCGAGGGGAACTTTAACGAAGCCGG + CACCGAACTCAGCCCTTTCACTTCTGG'3

Figure 6 shows where the guide RNA sequences target the *Mn1* locus, and the *Cas9* enzyme shall carry out the double-strand DNA cut. The sgRNA1 targets the first part of exon 1, the coding sequence of the gene. Such cut may result in a spectrum of changes, from producing transcript that undergoes nonsense-mediated decay or reading-frame shift, all possibly influencing the gene function. The location of sgRNA2 is at the beginning of the intron, the non-coding sequence spliced during the transcript processing. Deletions in this gene region may influence the splicing process and lead to differences in gene function. Combining the two sgRNAs in the dsRNA (double-guide RNA) plasmid shall result in the removal of the whole exon 1 of the *Mn1* gene.

Figure 6: schema of positions where the sgRNAs target the Mn1 locus

2.3.2. Transfection

In general, transfection introduces nucleic acids into eukaryotic cells with nonviral, chemical, or physical methods. Therefore, charged molecules such as plasmid-DNA need to overcome the hydrophobic part in the lipid bilayer of the cell membrane [28]. In this case, the cationic lipid reaction reagent Lipofectamine 2000 from Invitrogen; Thermo Fisher was selected. This reagent contains lipid subunits that form liposomes in an aqueous milieu. The liposomes entrap the plasmid DNA and transport it through the cell membrane [28,29]. The manufacturer claims the product's low toxicity and high efficiency, which should result in a high survival rate and a high proportion of transfected cells [29].

Because the plasmid contains a sequence of the 2A-GFP protein, successfully transfected cells produce the fluorescent protein and can be sorted using fluorescence-activated cell sorting (FACS).

2.3.3. FACS

Since transfection efficiency was only around 5 % (assessed by microscopy), and each transfected cell is likely to acquire distinct perturbation, GFP-expressing cells were sorted into the wells as single cells to avoid colonies of mixed genotypes. The droplet-based cell sorter produces a stream of single-cell-droplets via high-frequency vibration of the nozzle at an optimal amplitude over a certain period. Afterwards, every cell in the droplet passes through laser beams of focused light. Light scattering and fluorescence emission provide information about each of the cells. When a cell in a droplet matches the set of parameters defined by the FACS-operator, for example, being live, single and GFP-positive, such cell/droplet is given a charge and redirected into a collection tube or well [30].

The whole procedure and the absence of cell-to-cell contact after sorting are stressful for the cells. Therefore, a particular medium is required so that many cells recover and grow. The medium in which a particular cell line grew for a specific time is called a conditioned medium. The medium contains factors secreted by this cell line and can be used to stimulate the growth of the freshly sorted cells. A mixture of conditioned medium and fresh culture medium contains factors that promote the growth of the single cells.

2.3.4. Genotyping

Genotyping is a method for determining sequence differences in DNA collected from samples, such as cells or tissues.

The genotyping is performed by amplifying the region of interest using a specific set of primers - polymerase-chain-reaction (PCR) and subsequently assessed by the agarose-gel-electrophoresis.

The PCR amplification in a thermocycler is divided into three phases: denaturation, annealing, and elongation. It requires a DNA template, a thermostable DNA-polymerase, a specific buffer, deoxynucleoside triphosphates (dNTPs), and forward (FW)/reverse (RV)-primers. The first step of this process is the denaturation of the double-stranded template DNA. Next, the primers anneal at the beginning of the sequence that is going to be analysed. Finally, the DNA-polymerase incorporates the dNTPs complementary to the template DNA. This procedure is repeated for 20 – 40 cycles [31].

Agarose gel electrophoresis separates charged molecules, such as proteins or nucleic acids, in an electric field. The principle is based on the fact that DNA is negatively charged, and agarose gel has a lattice structure. An electric field is applied to the agarose gel and the DNA is placed on the opposite side of the anode into the wells of the gel. The negative DNA is then drawn through the gel to the positive charge of the anode. Amplified DNA molecules of diverse sizes exhibit different speeds within the gel. The pores of the gel offer less resistance to smaller fragments, which travel much faster to the anode than large DNA fragments [32].

The primers are designed to generate amplicons of desired sizes that allow distinguishing various genotypes on a gel. The primers were designed to validate whether major sequence perturbation (removal of the majority of exon1) is present in each expanded clone transfected initially with dgRNA construct (Figure 7).

The sgRNAs cause small deletions that do not significantly change the length of the amplicons; therefore, the bands on the gel would overlap and will not allow assessing the genotype. To assess the clones generated using sgRNA plasmids, sequencing is necessary.

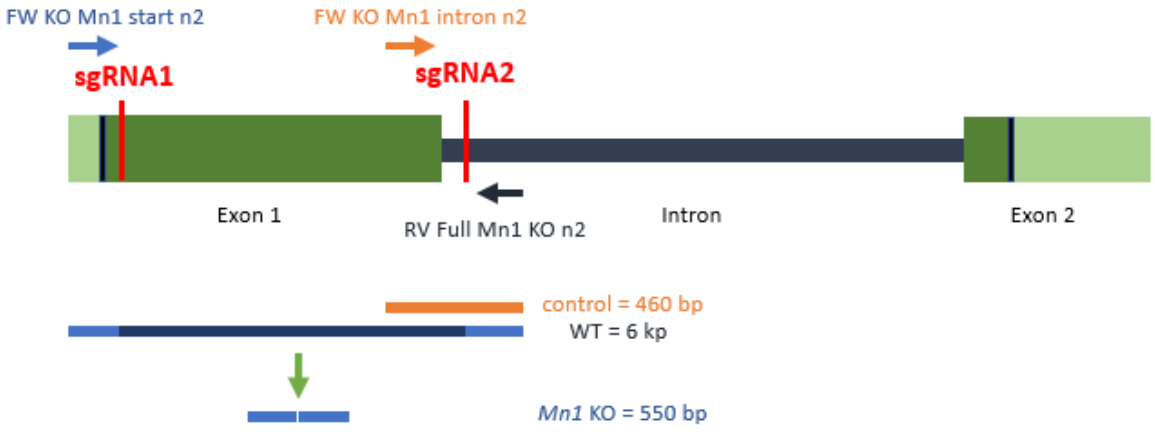

Figure 7: schema location of Primers used for genotyping

2.4. Differentiation and staining

Cell differentiation is the process in which cells specialise in their structure and functions. In the initial stage, the stem or progenitor cell has the potential to become one of a variety of possible cell types. While the actual multipotency is limited to embryonic stem cells (specifically, the cell of the inner cell mass), the repertoire of possible differentiation outcomes narrows down with every cell specification or fate decision. The differentiation affects the cell in its morphology and function. Cell differentiation is the outcome of various mechanical or molecular stimuli that are spatially and temporally coordinated [33].

The *in vitro* stimulation of cells can be performed by adding specific components to the cell culture medium. For the osteogenic differentiation of MC3T3- E1 cells *in vitro,* the *American Type Culture Collection* recommends adding a combination of β-glycerophosphate and ascorbic acid to the culture medium, comprising α-MEM, FBS, and antibiotics. The β-glycerophosphate is a phosphate donor required for the mineralisation of differentiating osteogenic cells. The ascorbic acid, commonly known as vitamin C, is essential for the maturation and deposition of collagen, and it contributes to the activity of the enzyme alkaline phosphatase (AP) [34].

The *in vitro* and *in vivo* differentiation of osteoblasts (including the MC3T3-E1) are classified into three phases: cell proliferation, matrix maturation, and matrix mineralisation. Each phase can be characterised by specific molecules or markers. During proliferation, cells start to produce various extracellular matrix proteins such as procollagen I, TGF-β, and fibronectin. While matrix maturation, the AP enzyme is at its peak of expression. At the beginning of matrix mineralisation, several other signalling molecules and markers, such as osteocalcin, osteopontin, and bone sialoprotein are expressed. In the mineralisation phase, the production of calcium, the bone stabilising vital mineral, marks the final step of osteogenic differentiation. The detection and analysis of the levels of such bone differentiation-specific markers are frequently used to characterise osteoblasts *in vitro*. Analysing methods include BCIP/NBT and Alizarin Red S (ARS) stainings for differentiation markers such as AP and Calcium [35].

2.4.1. BCIP/NBT staining

BCIP/NBT is the abbreviation for 5-bromo-4-chloro-3-indolyl-phosphate/nitro blue tetrazolium. It is an insoluble substrate that turns blue-violet in the presence of the enzyme alkaline phosphatase. The reaction is triggered by AP-catalysed dephosphorylation of BCIP, which converts NBT to the blue-violet NBT formazan. The higher the AP concentration is, the higher the colour intensity of the staining is noted. The colouration can be observed visually and is very stable and resistant to exposed light [36].

2.4.2. Alizarin Red S staining

Calcium can be detected by staining with Alizarin Red S. This water-soluble sodium salt of alizarin sulfonic acid has been widely used to evaluate calcium deposits in cell culture. According to chemical data ARS can react with Calcium through its sulfonic acid and/or its OH groups [37].

As with the BCIP/NBT staining, the more Calcium is produced, the more intense the staining gets. This staining is quite versatile because it can be observed visually, but also the ARS-bound Calcium can be extracted from the stained monolayer of cells and quantified. One assay for quantification is by extraction with a cetylpyridinium chloride (CPC) solution and analysis in a plate reader [38].

Since matrix mineralisation with Calcium production marks the phase of matrix maturation, the calcium concentration should increase after a high level of AP is already detectable. With these two staining methods, two phases of the differentiation process can be detected in order.

3. Materials and Methods

3.1. Targeted genome-editing of eukaryotic cells

3.1.1. Transfection

The MC3T3-E1 cells (Subclone 4; Culture Collections, Public Health England) were cultured in a medium composed of Dulbecco's Modified Eagle's Medium (DMEM + L-Glutamine, + 2.438 g/L Sodium Bicarbonate; HyClone™; Cytiva) containing 10 % fetal bovine serum (FBS; PAN-Biotech™) and 1 % antibiotic solution containing Penicillin and Streptomycin (Pen Strep; Gibco™; Life Technologies™) in a humidified 5 % CO_2 atmosphere at 37 °C (incubator; Sanyo MCO-18AIC(UV) CO2 Incubator).

The CRISPR/*Cas9*-constructs were introduced into the cells with the transfection reagent Lipofectamine 2000 (Invitrogen; Thermo Fisher Scientific).

Table 2: transfection reagents

construct	**well-plate-size**	**seeded cells**	**medium**	**Lipo. volume**	**amount DNA**	**OPT-MEM**
plasmid sgRNA1	6	0.5 x 10^6	2 ml	4.5 µl	1.5 µg	250 µl
plasmid sgRNA2	6	0.5 x 10^6	2 ml	4.5 µl	1.5 µg	250 µl
plasmid dgRNA	24*	1 x 10^5	0.5 ml	1.5 µl	0.5 µg	50 µl

* Due to the low concentration of the plasmid, this transfection was performed in a smaller well-size

One day before transfection, cells were seeded in the well plates (TPP®) with high density (see Table 2), so the cells were high confluent on the day of transfection. They were cultured in antibiotic-free DMEM/ F12 + 10 % FBS. It is essential that the medium does not contain any antibiotics during transfection; otherwise, the cell survival rate drops. The transfection complexes for individual wells were prepared as follows: First, the plasmid DNA and Lipofectamine 2000 were diluted in 125 µl/ 25 µl Opti-MEM (Gibco) and mixed gently. After 5 min incubation, the diluted DNA was added to the diluted Lipofectamine, mixed gently, and incubated for 15 min. Then the whole volume of 250 µl/ 50 µl was added to each well. The cells were kept at 37 °C in a 5 % CO_2 atmosphere. One day after transfection, the medium was exchanged for DMEM containing 10 % FBS and 1 % antibiotics (PenStrep). Then the transfected cells were observed using a confocal microscope (ZEISS LSM 980 Airyscan 2) to estimate the transfection efficiency.

3.1.2. FACS

The transfected cells were sorted as single cells into individual wells using FACS. In preparation for sorting, the transfected cells were detached from the surface after enzymatic treatment using trypsin and collected into a tube containing FBS to quench the enzymatic reaction. Cells were centrifuged at 1000 rpm for 5 min and resuspended in 1 ml DMEM based culture medium. To prevent the cell sorter from clogging, the cells must be separated. Therefore, the cells were filtered through a 12 x 27 mm cell strainer (FALCON®) and diluted in the culture medium in a total volume of 3 ml.

The transfected GFP-positive cells were sorted as single cells into two 96-well plates (Costar®). The wells contained 200 µl of the prepared single-cell medium, composed of 50 % conditioned medium and 50 % DMEM supplemented by 20 % FBS and 1 % antibiotics (PenStrep). The sorting was carried out using the BIO-RAD S3e™ Cell Sorter. The cell sorter separates heterogeneous cells according to a defined set of parameters. These parameters were set to sort alive, single, and GFP-positive cells. The gate settings for such a procedure are provided as supplementary information (attachment 0).

A few cells were sorted into a 1.5 ml tube and assessed under the confocal microscope to validate the credibility of the parameters and the cell sorting of the desired cell population.

After sorting, the cells were incubated at 37 °C in a 5 % CO_2 atmosphere.

On the 7th day of incubation, each well of the 96-well-plates was analysed under a confocal microscope, and the medium of wells with no cells was discarded. The wells with grown cells were counted and divided by the total number of wells used for the sorting (192 wells) to measure how many cells did recover and grow.

When the cells reached 50% confluence, they were transferred into 24-well-plates into DMEM containing 10% FBS and 1% Pen Strep.

3.1.3. Genotyping

For further analysis, 24 of the clones of each plasmid were selected. When the clones reached 90-100% confluency in the 24 wells, 1/3 of each clone was transferred into fresh 24-well-plates. The remaining 2/3 were transferred into 1.5 ml tubes. This procedure was repeated when the cells reached the desired confluency to secure enough material for DNA isolation. The cell samples in the 1.5 ml were spun down in a centrifuge (accuSpin Micro 17R; Fisher Scientific™) at 2500 rpm for 5 minutes, and the medium was discarded. Identical cell samples with the same label were resuspended together in 200 µl PBS and 20 µl Protease K was added. To extract the DNA, a DNeasy® Blood & Tissue Kit (Qiagen) was used. This kit utilises a DNA binding spin column and several cleaning steps, followed by a final elution to collect the DNA in a reaction tube, which was proceeded in 20 µl mqH_2O.

To measure the amount of extracted DNA the NanoDrop® ND-1000 Spectrophotometer (Peqlab Biotechnologie) was used.

The 24 DNA probes of the clones containing the dgRNA plasmid, were genotyped by PCR amplification of a specific region induced by specifically designed primers (Table 3) and subsequently assessed by agarose-gel-electrophoresis.

Table 3: PCR reagents

component			**volume per sample**
mqH_2O			12.8 µl
10X Dream Taq Green Buffer (Thermo Fisher Scientific)			2 µl
dNTP Mix (Thermo Fisher Scientific)			2 µl
FW Primer (Sigma-Aldrich)			1 µl
plasmid dgRNA	FW KO Mn1 start n2	5'-CTG TCA TGC CCT ATT GAT CC-3'	
control	FW KO Mn1 intron n2	5'-TTG AAA ATG GAG TTG GAC GG-3'	
RV Primer (Sigma-Aldrich)			1 µl
plasmid dgRNA	RV Full Mn1 KO n2	3'-AAG TCT CTA ACT CCT CAC ACC-5'	
control	RV Full Mn1 KO n2	3'-AAG TCT CTA ACT CCT CAC ACC-5'	
Dream Taq DNA Polymerase (Thermo Fisher Scientific)			0.2 µl
DNA			70 ng

The PCR was carried out in a Biometra TOne PCR Thermocycler (Analytic Jena GmbH) with the parameters presented in Table 4.

Table 4: Settings of the Thermocycler

step	temperature [°C]	time [min:sec]	procedure
1	93.0	03:00	prewarming
2	94.0	00:15	denaturation
3	62.0	00:20	primer annealing
4	72.0	00:30	elongation
30x cycles of steps 2 – 4			
5	72.0	05:00	final elongation
6	12.0	∞	storage

Afterwards, the agarose-gel-electrophoresis was performed. Therefore 10 µl of PCR-product were mixed with 2 µl loading buffer (6X TriTack DNA Loading Dye; Thermo Fisher Scientific) and added to a 1 % agarose gel (Sigma-Aldrich) in 1X TEA buffer (Roth). The electrophoresis was running for 40 min at 90 volts (BIO-RAD).

The gel was analysed in a Molecular Imager® Gel Doc™ XR+ with Image Lab™ Software (BIO-RAD).

3.2. Differentiation and staining

For differentiation and staining, the MC3T3-E1 cells were cultured in a medium composed of α-minimal essential medium (α-MEM +L-Glutamine, +Ribonucleosides, and Deoxyribonucleosides; HyClone™; cytiva) containing 10 % FBS and 1 % antibiotic solution (PenStrep) in a humidified 5 % CO_2 atmosphere at 37 °C.

The cells were seeded into 24-well plates (TPP®) at a 2.5 x 10^4 cells/ well density. When cells reached 70% confluency, the culture medium was replaced by the α-MEM-based differentiation medium. The differentiation medium further comprised 50 µg/ml of ascorbic acid and 10 mM β-glycerol phosphate. The differentiation medium was freshly prepared and changed every second to third day throughout the experiment. Cells were cultured in the standard culture medium without additives to secure negative control. For each staining, three technical triplets were prepared.

3.2.1. Detection of alkaline phosphatase (BCIP/NBT staining)

For the detection of AP, the cells were stained with BCIP/NBT (SigmaFast™; Sigma-Aldrich) after 7, 10, and 14 days in the differentiation medium. Before starting the staining, all solutions needed were prepared. Therefore, a BCIP/NBT tablet was dissolved in 10 ml of sterile MilliQ water (mqH_2O). The solution must be stored in the dark and used within two hours. For the washing buffer, 5 µl Tween® 20 (Life Science; Sigma-Aldrich) was added to 10 ml Dulbecco's Phosphate-Buffered Saline w/o Ca++/ Mg++ (DPBS; PAN-Biotech™).

The first step of the staining was washing the cells twice with DPBS without disrupting the cell monolayer. Then the cells were fixed for 30 – 40 seconds with cold 4 % Paraformaldehyde (PFA; Sigma-Aldrich). It is important not to fix the cells for longer than 60 seconds, otherwise, the fixation will lead to irreversible inactivation of the AP. Subsequently, the cell monolayer was washed twice with the washing buffer. Afterwards, the cells were incubated with 500 µl BCIP/ NBT substrate solution at room temperature in the dark. After 10 min incubation, the cells were washed twice with washing buffer. For analysing the results under an inverse phase-contrast microscope (Leica DM LB), the washing buffer was displaced with 500 µl DPBS. Pictures were taken with a camera adapted to the microscope (Leica EC3).

3.2.2. Detection of Calcium (Alizarin Red S staining)

Detection of Calcium was performed by Alizarin Red S (ARS). To prepare the ARS staining solution, 0.6 g of ARS powder (Roth) were dissolved in 30 ml sterile mqH_2O, and the pH was adjusted to 4.1 – 4.3. The solution was stored in the dark at 2 – 8 °C (fridge; Liebherr).

For the staining, the cells were removed from the incubator and washed twice with DPBS. Then cells were fixed for 10 min in cold 4 % PFA and washed three times with mqH_2O. Immediately before use, the ARS staining solution was filtered through a 0.22 µm filter membrane (Roth). After aspirating the mqH_2O, 300 µl filtered ARS staining solution was added to cover the cell monolayer and incubated in the dark at 37 °C for 30 min. Then the cells were washed five times with mqH_2O and analysed using an inverse phase-contrast microscope (Leica DM LB) in 500 µl DPBS. For documentation of the results, pictures were taken with a camera adapted to the microscope (Leica EC3).

To quantify this staining in a plate-reader, the Alizarin Red S-stained cells were incubated with 400 µl of 10 % cetylpyridinium chloride (CPC, Hexadecylpyridinium Chloride Monohydrate, Tokyo Chemical Industry) dissolved in a 10 mM sodium phosphate buffer (pH 7). As result, the calcium-bound ARS was released into the solution. After 15 minutes of incubation, 200 µl/ well of the solution was transferred to a 96-well plate. The absorbance was measured at 562 nm using a microplate reader (Infinite M Nano+; Tecan).

To determine the Alizarin Red S concentration in millimole (mM), a standard curve was prepared (see Table 5 and Figure 8).

Standard curve: stock solution = 2 % ARS

Table 5: Preparation data for the standard curve

step	dilution	procedure	ext. [-] *M* minus Blank	molarity ARS [mM]
1.	1/125	24 µl stock solution + 2976 µl of 10 % CPC	1.4183	0.0467
2.	3/4	1500 µl from 1. + 500 µl of 10 % CPC	1.0749	0.0350
3.	1/3	333 µl from 2. + 667 µl of 10 % CPC	0.3694	0.0117
4.	1/4	350 µl from 3. + 1050 µl of 10 % CPC	0.0949	0.0029
5.	1/2	550 µl from 4. + 550 µl of 10 % CPC	0.0474	0.0015
6.	1/2	400 µl from 5. + 400 µl of 10 % CPC	0.0225	0.0007
7.	Blank	10 % CPC	0	0

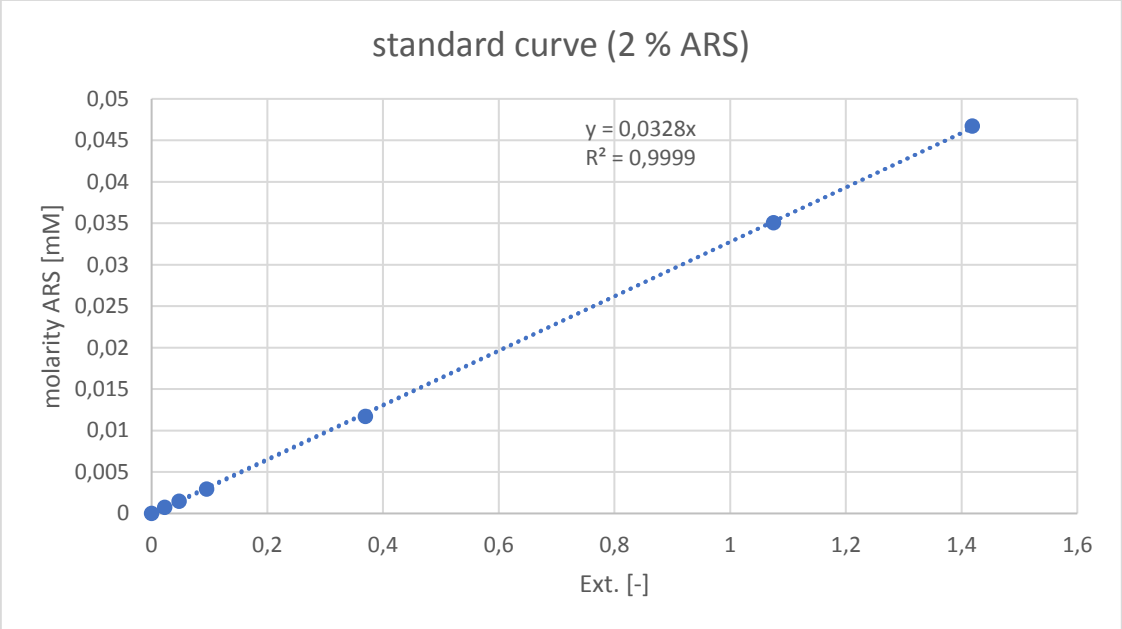

Figure 8: standard curve of 2 % Alizarin Red S dissolved in 10 % Cetylpyridinium chloride measured at 562 nm

4. Results and discussion

4.1. Targeted genome-editing of eukaryotic cells

The first step of the targeted mutation process was the transfection of the CRISPR/Cas9 plasmids with Lipofectamine 2000.

The cells were analysed under a confocal microscope 24 hours after transfection (Figure 9). Based on the resulting fluorescence scans and brightfield images, transfection efficiencies were determined (Table 6). Since the cells were overgrown and not explicitly countable, the number of alive cells is vague.

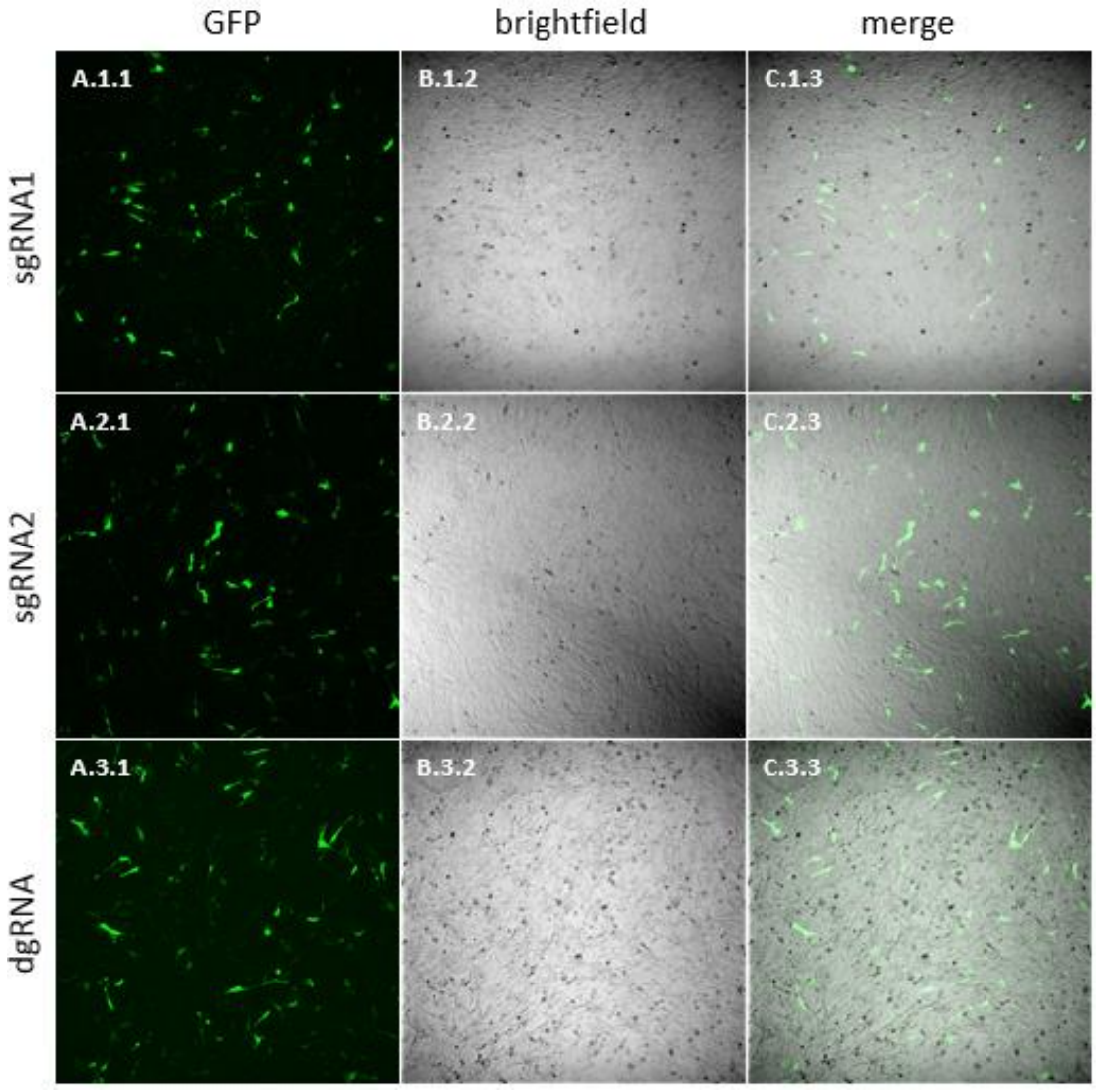

Figure 9: Transfected MC3T3-E1 after 24 h under a confocal microscope (lens 10x), (A) detect GFP-signal of transfected cells using laser beams, (B) cells viewed in a brightfield to measure the number of alive/ dead cells, (C) composition of both settings; (1) cells transfected with plasmid sgRNA1, (2) cells transfected with plasmid sgRNA2, (3) cells transfected with plasmid dgRNA

All three samples had a decent proportion of cells with a clear GFP signal showing the plasmids were successfully transfected, but the contracted shape of the fluorescent cells did indicate some level of cell stress. The black round spots visible in the brightfield images are, in fact, dead cells. A high value of dead cells also indicates a high stress level. This shows that Lipofectamine 2000 had a cytotoxic effect on the cells. Most dead cells were in the sample of the transfected cells with the dgRNA plasmid. This might be because these cells were transfected in a different well size with a different concentration of Lipofectamine and DNA than the other two. The cell sample transfected with sgRNA1 also contained a significant proportion of dead cells, but less than in the dgRNA sample. The most viable cells, which also had the fittest morphology, were the plasmid sgRNA2 transfected cells.

Table 6: Transfection Efficiency

plasmid	**GFP positive cells/alive cells**	**efficiency [%]**
plasmid sgRNA1	28/ ~2000	~1,4
plasmid sgRNA2	44/ ~2500	~1,76
plasmid dgRNA	75/ ~2000	~3,75

The highest transfection efficiency had the cells transfected with the dgRNA plasmid. Since this sample also contained most dead cells, it shows that the relation between Lipofectamine, DNA, and cell number per area influences the transfection efficiency. Concerning the cell number, the Lipofectamine and DNA concentrations were higher in the 24-well than in the 6-well. On the one hand, Lipofectamine had the highest toxicity with the 24-well condition, but on the other, it was the most efficient condition of plasmid intake.

After it was determined that the transfection was successful, the cells were sorted by FACS. To verify the sorting protocol, some GFP positive single cells were collected in a 1.5 ml tube after the parameters for the cell sorting were set. The cells were analysed using microscopy (Figure 10).

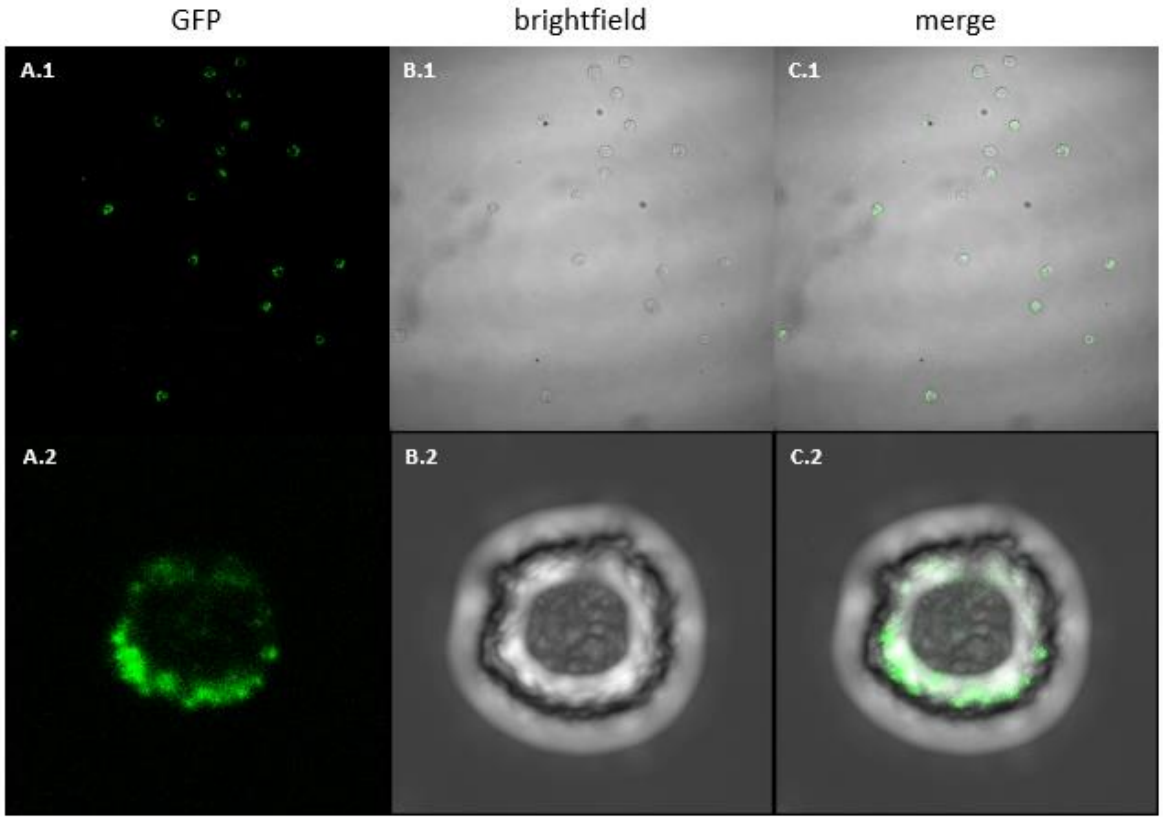

Figure 10: Sorted MC3T3-E1 transfected after 24 h under a confocal microscope, (A) GFP, (B) Brightfield, (C) Composition, (1) upper row shows the cells in a 10 X lens, (2) bottom row shows a close-up of one cell

It can be seen in the brightfield (B), that the cells were individual and undamaged. The sorted cells were GFP positive, as visible in the combination picture (C.2). This shows that living, single, GFP-positive cells were sorted. Image C.2 shows that the GFP signal came from inside the cell.

The sorted cells were allowed to grow for 7 days. Then each well was checked to see if it contained clones (Table 7).

Table 7: count of wells with grown cells in 96-well-plates after 7 days

plasmid	**grown clones/ 192 wells**	**efficiency [%]**
plasmid sgRNA1	47/192	25
plasmid sgRNA2	72/192	38
plasmid dgRNA	56/192	29

Some clones grew in the single-cell medium composed of a conditioned medium and culture medium. With a survival of 38% after cell sorting, the cells transfected with plasmid sgRNA2 were recovering and growing the most. This might be related to the fact that these cells were in the fittest shape after transfection (Figure 9). The lowest number of viable and growing cell colonies were detected in the sgRNA1 transfected cells. This could have been because these had the least transfection efficiency and less viable cells than plasmid sgRNA2. With a clone survival rate of 29%, the dgRNA is between the other two. This condition expressed the lowest cell viability after transfection and the highest transfection efficiency.

When the clones reached a confluency of around 50%, they were transferred to 24-well-plates. Because the clones grew at different rates, they did reach the confluency on different days starting on day 10 after sorting. On the 14th day after, all clones were transferred into 24-well-plates and analysed for their shape by phase-contrast microscopy. To see whether the clones showed any differences in shape, the images were compared with images of the original MC3T3-E1 cells at different confluences (Figure 11).

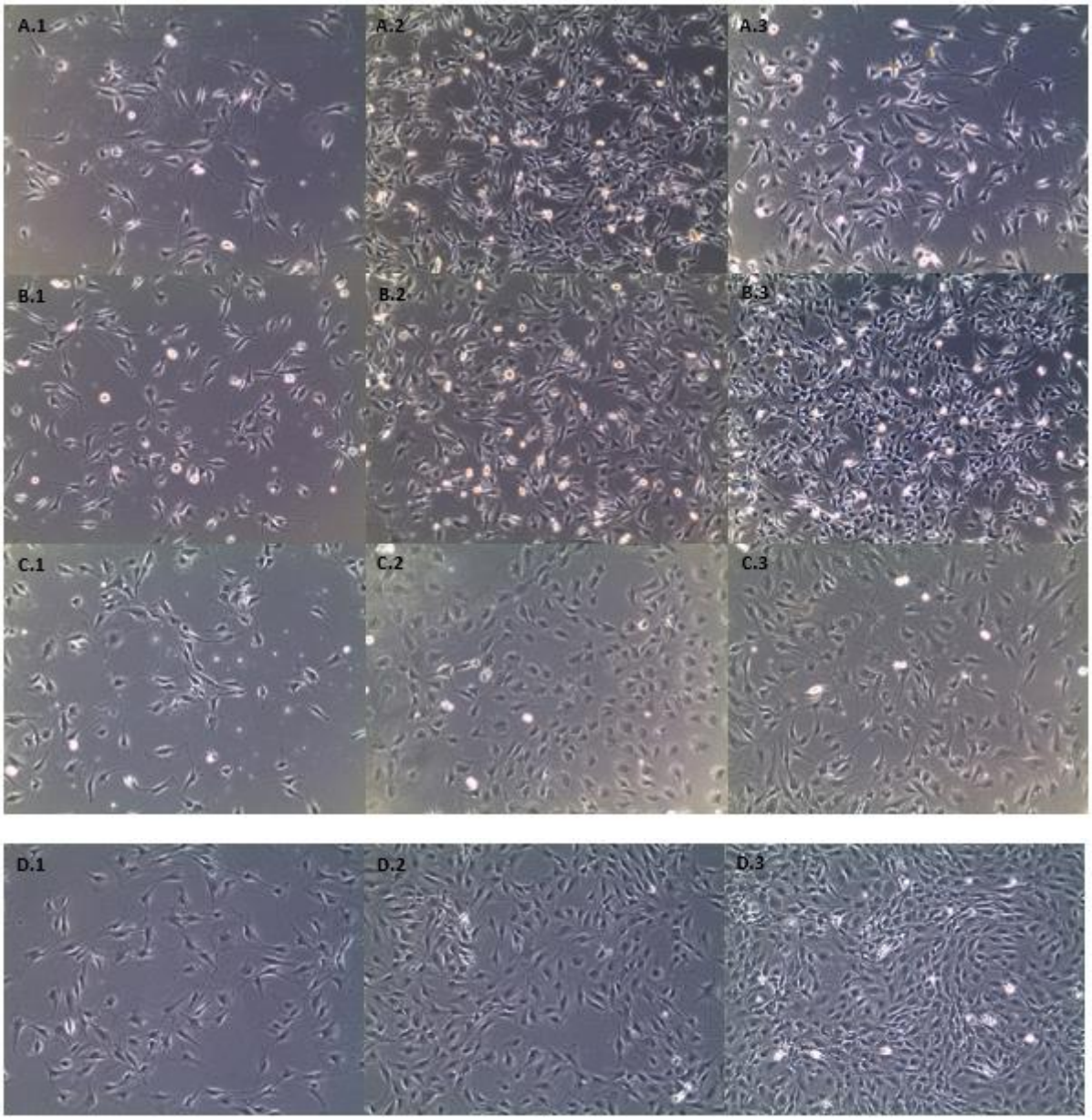

Figure 11: clones in 24-well-plates 14 days after sorting (A) clones that were transfected with plasmid sgRNA1, (B) clones with sgRNA2, (C) clones with dgRNA, (D) different confluences of the original MC3T3-E1

The images illustrate that the clones grew at different growth rates. This could have been influenced by stress during transfection and sorting or how fast they attached to the plate ground and recovered. The growth rate differences could also correlate with the severity of the mutation.

Compared to the original MC3T3-E1, the clones appeared to have several different morphologies. While changes in cell morphology may indicate successful mutations, they can also indicate cell stress.

When the cells reached a high confluence in the 24-wells, samples were taken for Genotyping. The isolated DNA was measured by Nanodrop. Table 8 shows examples of the Nanodrop values indicating the concentration and purity of extracted DNA. The complete Table of plasmid dgRNA and the tables of the other two plasmids are provided in the supplementary information (attachment 0).

Table 8: Nanodrop results of extracted DNA from clones transfected with plasmid dgRNA

Clone	λ [nm]	A-260 10 mm path	A-280 10 mm path	260/280	260/230	DNA [ng/µl]
4.1	230	0.788	0.391	2.02	1.01	39
4.2	230	0.326	0.182	1.79	0.62	16
4.3	230	0.888	0.392	2.27	1.92	44
4.4	230	0.811	0.375	2.16	1.08	41
4.5	230	0.653	0.275	2.37	1.27	33
4.6	230	0.795	0.380	2.09	1.31	40
4.7	230	2.462	1.201	2.05	1.77	123
4.8	230	0.782	0.422	1.85	1.11	39
4.9	230	0.721	0.354	2.04	1.41	36
4.10	230	0.920	0.441	2.08	1.24	46

The results show different concentrations of DNA ranging from 16.29 ng/µl to 123.11 ng/µl. Values correlate with the number of cells that the DNA was extracted from. The more cells were in the sample; the more DNA was extracted.

The absorbance ratios 260/280 and 260/230 give information about the purity of the DNA, as its absorbance is at 260 nm. Values of 1.8 at 260/280 ratios indicate that the samples are pure DNA. However, RNA also has an absorbance at 260 nm and has an optimal 260/280 ratio of 2.00 [39]. Most of the 260/280 ratios were around 2, which indicates a possible significant presence of RNA.

The 260/280 ratio is also an indicator of protein contamination because the absorbance for protein is at 280 nm. Values lower than 1.8 imply contamination by proteins. Since high protein contamination can inhibit applications such as PCR, samples with values less than 1.70 should be avoided [39].

An absorbance ratio of 260/230 less than 1.8 indicates contamination caused by organic compounds or chaotropic substances. The absorbance of these substances is at 230 nm [39].

Most of the ratios of the extracted DNA were significantly lower than 1.8. This implied high contamination by other substances. Most likely, these were remnants of ethanol used during the DNA isolation.

Of the isolated DNA 24 samples were analysed by PCR and agarose-gel-electrophoresis (Figure 12). These clones were initially transfected with the CRISPR/Cas9 and the dgRNA.

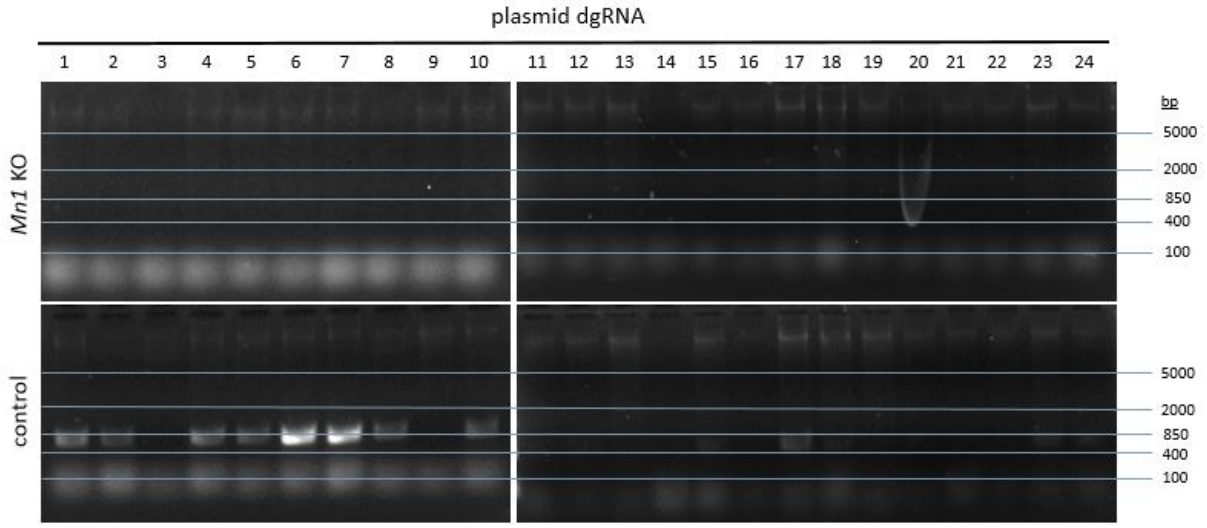

Figure 12: agarose gel electrophoresis from PCR of knock-out locus and control (plasmid dgRNA)

The two upper gels present the PCR results from the primers for the *Mn1* KO amplification. A band at 400 and 850 bp shall be detected if the deletion of exon 1 in *Mn1* was successful. In probe #20 a smear was visible, leading to the assumption of one positive clone. In all other clones was no sign of an *Mn1* KO band.

The control group did have some visible bands between 850 and 400 bp. Since the amplified sequence between the control primers shall result in 460 bp amplicon, we can be sure that we detected the proper control band. This indicates that the PCR worked at least for the probes with a clear band.

Probes with no bands in the *Mn1* KO and the extracted DNA control were probably not clean or concentrated enough for the PCR.

Since the PCR probe from clone 20 was ambiguous, the clone was amplified together with clones 19 and 21 in 6-well-plates to get more DNA, and the genotyping was repeated (Figure 13).

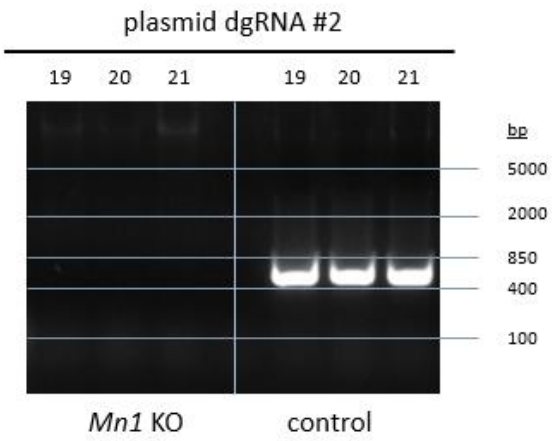

Figure 13: agarose gel electrophoresis from PCR of knock-out locus and control (plasmid dgRNA #2)

In this Figure on the left sight, the gel of the PCR with the primers for the *Mn1* KO, and on the right is the control group. The control shows clear bands between 850 and 400 bp, while in the *Mn1* KO no band was detected. This means that there was no successful mutant within the 24 selected clones with the deletion of exon 1 in the *Mn1* gene. What is noticeable when comparing the two images is that the bands are much clearer. Referring to the Nanodrop result the DNA was more concentrated and cleaner, because of the higher cell number in the samples that were grown in 6-well plates. This aspect shall be also considered for future genotype analysis of clones.

It may have happened that the CRISPR system did cut at one of the sgRNA locations and caused perturbations in the gene, but this must be analysed by sequencing (as the clones that contained plasmid sgRNA1 and 2). The genotyping of the remaining clones with the dgRNA and of the clones with the sgRNA1 and sgRNA2 was not performed. Therefore, whether genome editing was successful cannot be concluded.

The above-described procedure shows that the targeted perturbation production and assessment rely on many parameters.

First, the plasmid needs to be transported through the cell membrane without compromising the cell viability. The Lipofectamine 2000 was reasonably efficient, as a clear GFP signal was detected. For the CRISPR/Cas9-editing tool to succeed, it is necessary to know whether the construct is indeed expressed in the cell. The GFP protein signal indicated that the plasmid was expressed; therefore, it can be assumed that the other CRISPR/Cas9 components were expressed as well.

When the CRISPR system is implemented correctly, the sequence where the PAM and guide RNA match has to be recognised. This step can result in an off-target effect, which is defined as unintended cleavage and mutation at nontargeted genomic sites. These sites have a sequence that is quite similar but not identical to the target sequence [40].

This can lead to false results when mutations in other parts of the genome are responsible for different cell behaviour. Additionally, when single cuts were made, there is no guarantee that the repair mechanisms of the cell caused a mutation that affects the gene. The repair can be identical to the original gene, or changes do not cause an effect (silent mutations).

Since the CRISPR-System with dgRNA has to cut in two parts of the gene, it is even less likely that the cuts are made correctly, and the chance of acquiring the desired mutation is lower.

After transfection and establishment of the CRISPR system, the cells with a corresponding mutation must be sorted. The cells need to recover from the procedure and start to grow without initially having cell-to-cell contacts. Throughout this process, the cells must not be stressed too much, as this can change their behaviour and functions or cause natural mutations in other parts of the genome, which may lead to false results in the following experiments.

Going through the gates of the FACS parameters, it occurred that the settings were not set adequately. The first gate where alive cells were marked, was only measured by size and granularity. However, dead cells with a damaged membrane can exhibit autofluorescence, so this setting does not precisely assess the condition of the cell. Therefore, the FACS settings were optimised, and the experiment was repeated. To mark and sort out the dead cells, the dye Propidium Iodide (Abcam) was added to the cell suspension before sorting. This standard reagent is used for assessing cell viability in flow cytometry. It binds to double-stranded DNA but is unable to enter live cells with intact plasma membranes [41].

In addition, to decrease the stress during sorting by FACS, the cells were cooled and resuspended in isotonic buffer solution DPBS before the sorting process to lower their cell activity and metabolism. The new gates for this sorting are provided in the supplementary information (attachment 0). Currently, these cells are maintained and being expanded, and the validations will be performed in approximately four weeks.

4.2. Differentiation and staining

In the following section, the results of the differentiation and staining optimisation of the original MC3T3-E1 subclone 4 cells are presented. This setup will be used to functionally validate the introduced perturbation in the *Mn1*-mutants.

Figure 14 and Figure 15 show stainings of MC3T3-E1 passage 9 cells for alkaline phosphatase (figure x1) and Calcium (figure x2) after 7, 10, and 14 days in the differentiation medium. In the upper row of these figures, the stains are presented at low magnification. These images cover a large part of the stained well area and provide a solid overview of the AP and Calcium concentration differences at different time points of differentiation. The bottom row shows the stained cells in detail with higher magnification.

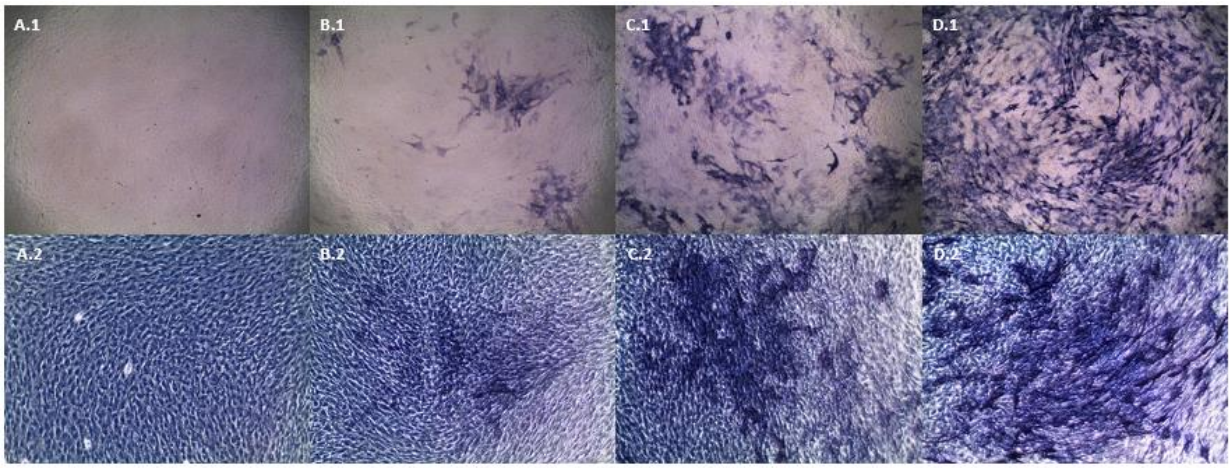

Figure 14: BCIP/NBT staining for alkaline phosphatase in MC3T3-E1 passage 9, control (A), after 7 days (B), 10 days (C), 14 days (D) of differentiation, (1) upper row, the stains presented with a 4 X lens, (2) bottom row, the stains presented with a 10 X lens

The images B – D in Figure 14 clearly show that the concentration of alkaline phosphatase increased with time in the differentiation medium. On day 7 (images B.1 and B.2) the AP concentration was quite low, which indicates that the matrix maturation phase starts around

this time point. As visible in images C.1 and C.2, the AP concentration is higher on day 10. The staining increased steadily and reached 80 – 90% of the area on day 14 (images D.1 and D.2).

As expected, in the control, no alkaline phosphatase was detected. This indicates that the differentiation medium and staining with BCIP/NBT work well for MC3T3-E1 subclone 4.

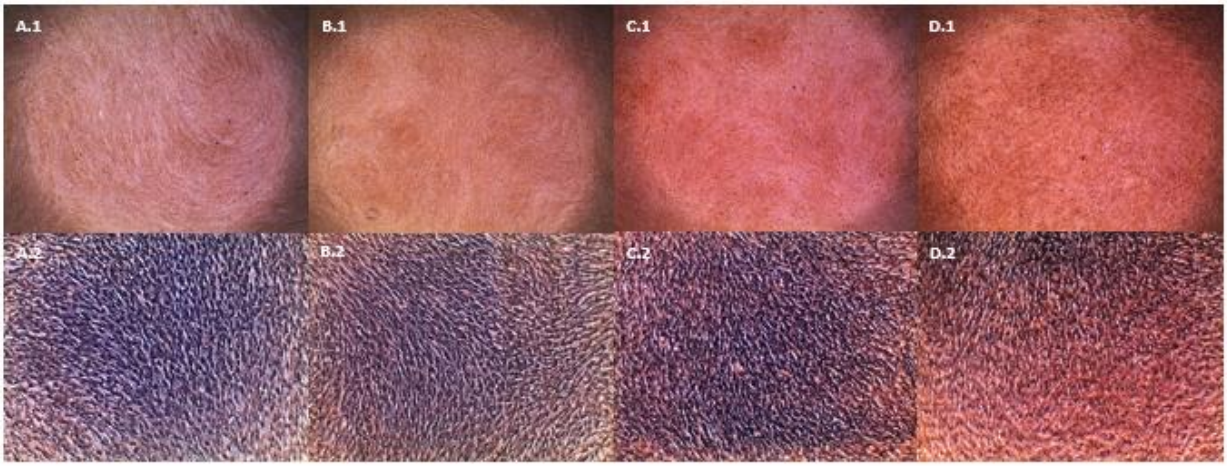

Figure 15: Alizarin Red S staining for Calcium in MC3T3-E1 passage 9, control (A), after 7 days (B), 10 days (C), 14 days (D) of differentiation, (1) upper row, the stains presented with a 4 X lens, (2) bottom row, the stains presented with a 10 X lens

As can be seen, in Figures B - D of Figure 13 for the ARS, the visible difference between days 7 and 14 of staining is not evident. The slight stain of the control group is as expected and can be considered as background. Compared to the control, the staining on day 7 (images B.1 and B.2) showed a minor, but no significant difference in Calcium concentration. On days 10 and 14 (images C.1 – D.2), the concentration of detectable Calcium was rising to a more notable level. This indicates that the matrix mineralisation slowly starts between day 10 and 14 but does not rise to an excessive concentration of Calcium. Nevertheless, it shows that the cells were differentiating.

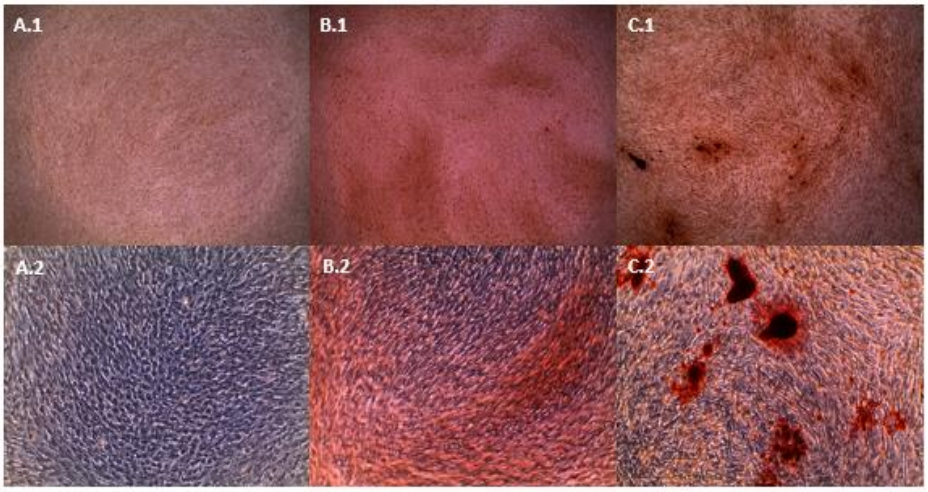

Figure 16: Alizarin Red S staining for calcium in MC3T3-E1 passage 6 control (A), after 14 days (B) and 21 days (C) of differentiation

A second staining for Alizarin Red S, but with passage 6 and on the differentiation days 14 and 21 was proceeded (Figure 16). As images A.1 – B.2 display, a visible difference in the Calcium concentration between control and the staining was detected on differentiation day 14. On day 21 (images C.1 and C.2), apparent mineralised nodules were detectable, clearly showing the extracellular matrix was mineralising. This indicates that the matrix mineralisation starts around day 14 and reaches a significant level around day 21.

Figure 15 compares the results of the ARS stainings from before in terms of their ARS molarities. These were calculated from the plate reader measurements of the ARS-bound calcium extractions with 10% CPC (attachment 0).

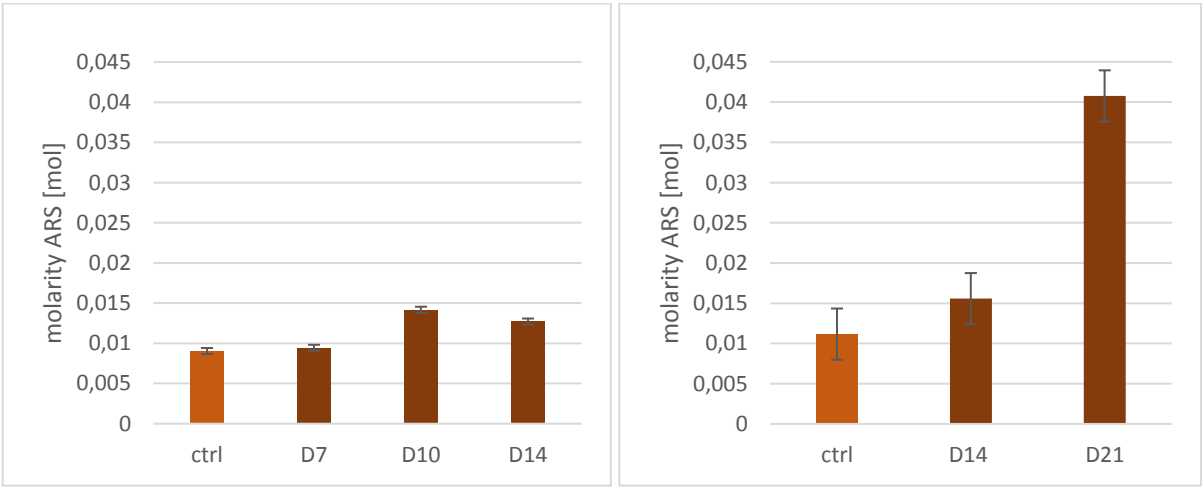

Figure 17: Mol concentrations of ARS-bound calcium after extracting with 10% CPC; (left) MC3T3-E1 passage 9 on day 7, 10 and 14; (right) MC3T3-E1 passage 6 on day 14 and 21

On the left are the molarities of the ARS stainings presented in Figure 15. As can be seen, the molarity of the control was the lowest with 0.00904 mol. The staining from differentiation day 7 shows slightly higher molarity with 0.00944 mol, but this is not significant compared to the control. This coincides with the images from this staining. Day 10 had the highest molarity out of these four with 0.01411 mol, and day 14 was with 0.01271 mol between 10 and 7. This is not in line with the expectation and the visible result in Figure 15. Because by comparing the images of these days, day 14 seems to be of a higher colour intensity than day 10. Perhaps the extraction with the CPC was not working correctly in that experiment.

The right diagram shows the molarities of the second ARS staining displayed in Figure 16. The mol concentration of the differentiation cells was at 0.01556 mol on day 14. The control sample had a molarity of 0.01115 mol, which is lower than the molarity in the differentiated cells. Compared to the control and the staining of day 7 in the other diagram, the molarity was higher. With 0.04075 mol the staining of differentiation day 21 showed a significantly high concentration of ARS-bound Calcium, matching the visible mineralisation nodules.

The results of both diagrams compared indicate that the Calcium production between differentiation days 7 and 14 was slowly starting and detectable, but not expressive. Subsequently, the Calcium production strongly increased and reached a significant level on the 21st day of differentiation. In summary, the results indicate that the ARS-staining with subsequent extraction with CPC is also working well for the MC3T3-E1.

Both stainings in combination give an expressive overview of the differentiation process.

The results of the two staining methods considered together matched the order of the differentiation phases. The second phase of the cell differentiation process – matrix maturation – is signalled by an increasing appearance of alkaline phosphatase between differentiation days 7 and 14. The subsequent matrix mineralisation is visible by the raising Calcium concentration. Between 10 to 14 days in the differentiation medium the cells were starting to produce low concentrations of Calcium and the phase transition is slowly being introduced. Then between the 14th and 21st day of differentiation, the Calcium is highly produced, and well recognizable mineralised nodules are built.

A comparison of BCIP/NBT staining and ARS staining at passage 6 (upper row) and passage 30 (bottom row) underlines the effect of cell age on differentiation (Figure 18).

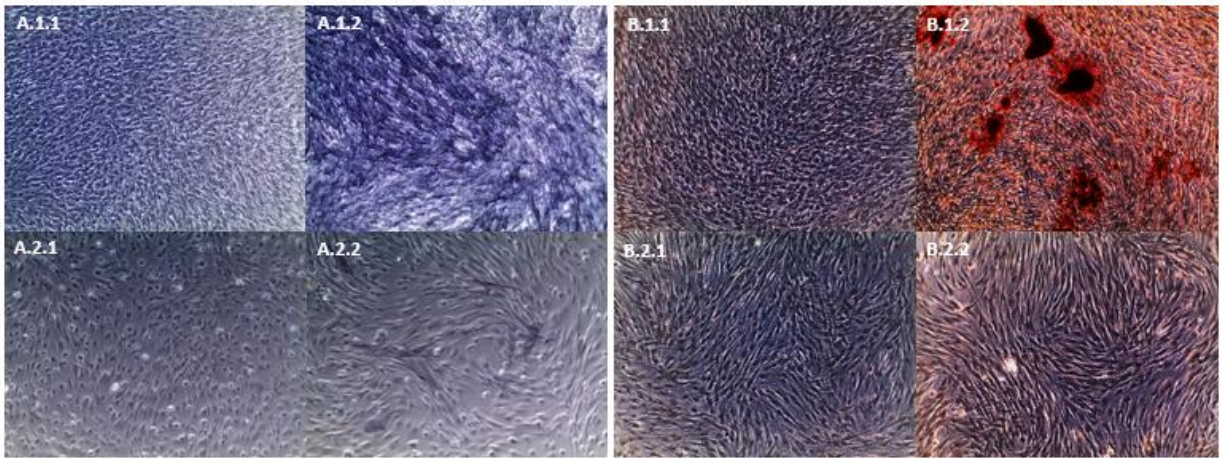

Figure 18: Effects of differentiation on passage 6 (upper row) and 30 (bottom row) of the MC3T3-E1 cell line (A) differentiation day 14, (B) differentiation day 21

The BCIP/NBT staining on the left was performed on day 14 of differentiation. The younger passage shows a clear, strong signal of detected alkaline phosphatase, while the signal in the older passage is comparatively weak.

The images on the right of an ARS staining on day 21 of differentiation also show that passage 6 has red-stained Calcium deposits, while there is hardly any colour difference in passage 30.

Additionally, there is a visible difference in the morphology and confluency of the cells. The young passage is highly confluent, with no space between cells. As seen in the old passage, the cells steadily slowed down dividing and still have space between them.

These results show the importance of using young passages and definitely should be considered in differentiation experiments with mutant cell lines. Because during procedures like establishing new lines, cells also grow older. Additionally, as the results of the gene-editing process show, the process is stressful for the cells, which also can influence their differentiation ability. Therefore, it is necessary to select cells that went through the same process and did not acquire mutation, as a control.

5. Summary

Even though the development of genome editing tools such as CRISPR/Cas-systems has made DNA modification easier and more effective than ever before, targeted mutation and the establishment of new cell lines depend on various parameters. They range from the efficiency of introduction of the CRISPR system into the cell, to cell-intrinsic DNA repair mechanisms, sorting and growth of the cells, and correct genotyping. In addition, throughout the establishment process, care must be taken that the cells do not become overly stressed, and excessively aged. Otherwise, cells might change physiology and function and acquire an additional mutation in other loci, leading to false results in the subsequent investigation.

To this date, no successful mutation in the *Mn1* gene of the MC3T3-E1 clones has been validated by genotyping. According to the interim results, transfection and sorting were successful, and colonies established from the single cells were able to grow. However, the cells exhibited shapes indicative of stress.

The original MC3T3-E1 (without targeted modifications in the *Mn1* locus) was successfully differentiated in a culture medium supplemented with ascorbic acid and β-glycerophosphate. Using the BCIP/NBT staining method, an increasing concentration of AP was detected, starting on differentiation day 7. On day 14, the staining of the cell monolayer was between 80% and 90%. Also, Calcium was detected by using Alizarin Red S staining, and the concentration was measured in a plate reader after extraction with CPC of the ARS-bound Calcium. The stainings did show that the calcium expression started between differentiation day 10 and 14 and increased strongly afterwards. On day 21, the cells contained a high Calcium concentration, both staining and plate-reader measurements confirmed that. During differentiation AP, marks the matrix maturation and Calcium is a hallmark of the subsequent matrix mineralisation. The order in which increasing concentrations were detected matches the phases of differentiation. In addition, a comparison of different passages highlighted the effect of passage number (as an equivalent of ageing) on the capacity to differentiate (passage 30 cells could not be differentiated).

6. Outlook

When new cell line clones with either minor perturbation or the deletion of exon 1 of the *Mn1* gene are successfully established, the differentiation and stainings will allow to functionally validate the function of *Mn1*. The expectation is that the deletion or other perturbations affect the differentiation ability of the cells. This will allow to reveal the function of this gene in osteoblast growth, differentiation, and physiology. Moreover, other assays such as MTT can be applied to these mutants to see how the introduced perturbation affects other functions of the cells.

Additional further investigations of *Mn1* in other organisms such as mice, chicken embryos, and sharks will clarify the function of this gene in the development and the evolution of the vertebrate head.

7. Dedication and acknowledgement

I would like to thank Dr. Marketa Kaucka Petersen for the possibility to work in her research group. In addition, I also want to thank her and all the members of the group for all the support during my time at the institute.

Also, I would like to thank the Max Planck Society for providing work space and resources for my reasearch.

Special thanks go to Prof. Dr. Holger Rehmann for supervising my thesis and always having the time to help and answer questions.

8. References

[1] A.P. Murillo-Rincón, M. Kaucka, Insights Into the Complexity of Craniofacial Development From a Cellular Perspective, Front. Cell Dev. Biol. 8 (2020) 1–8. https://doi.org/10.3389/fcell.2020.620735.

[2] B. Hallgrimsson, W. Mio, R.S. Marcucio, R. Spritz, Let ' s Face It — Complex Traits Are Just Not That Simple, PLoS Genet. 10 (2014) 10–12. https://doi.org/10.1371/journal.pgen.1004724.

[3] C.P. Klingenberg, Evolution and development of shape: integrating quantitative approaches., Nat. Rev. Genet. 11 (2010) 623–635. https://doi.org/10.1038/nrg2829.

[4] W.R. Atchley, B.K. Hall, A model for development and evolution of complex morphological structures., Biol. Rev. Camb. Philos. Soc. 66 (1991) 101–157. https://doi.org/10.1111/j.1469-185x.1991.tb01138.x.

[5] S.W. Jin, K.B. Sim, S.D. Kim, Development and growth of the normal cranial vault: An embryologic review, J. Korean Neurosurg. Soc. 59 (2016) 192–196. https://doi.org/10.3340/jkns.2016.59.3.192.

[6] NCBI, Mn1 meningioma 1 [Mus musculus (house mouse)], (2022). https://www.ncbi.nlm.nih.gov/gene?Db=gene&Cmd=DetailsSearch&Term=433938. (02.04.2022)

[7] NCBI, MN1 MN1 proto-oncogene, transcriptional regulator [Homo sapiens (human)], (2022). https://www.ncbi.nlm.nih.gov/gene/4330. (02.04.2022)

[8] T.B. Davidson, P.A. Sanchez-Lara, L.M. Randolph, M.D. Krieger, S.Q. Wu, A. Panigrahy, H. Shimada, A. Erdreich-Epstein, Microdeletion del(22)(q12.2) encompassing the facial development-associated gene, MN1 (meningioma 1) in a child with Pierre-Robin sequence (including cleft palate) and neurofibromatosis 2 (NF2): A case report and review of the literature, BMC Med. Genet. 13 (2012) 19. https://doi.org/10.1186/1471-2350-13-19.

[9] J. Breckpot, B.M. Anderlid, Y. Alanay, M. Blyth, A. Brahimi, B. Duban-Bedu, O. Gozé, H. Firth, M.C. Yakicier, G. Hens, M. Rayyan, E. Legius, J.R. Vermeesch, K. Devriendt, Chromosome 22q12.1 microdeletions: Confirmation of the MN1 gene as a candidate gene for cleft palate, Eur. J. Hum. Genet. 24 (2016) 51–58. https://doi.org/10.1038/ejhg.2015.65.

[10] R.H. Lekanne Deprez, P.H. Riegman, N.A. Groen, U.L. Warringa, N.A. van Biezen, A.C. Molijn, D. Bootsma, P.J. de Jong, A.G. Menon, N.A. Kley, Cloning and characterization of MN1, a gene from chromosome 22q11, which is disrupted by a balanced translocation in a meningioma., Oncogene. 10 (1995) 1521–1528.

[11] A. Buijs, S. Sherr, S. van Baal, S. van Bezouw, D. van der Plas, A. Geurts van Kessel, P. Riegman, R. Lekanne Deprez, E. Zwarthoff, A. Hagemeijer, Translocation (12;22) (p13;q11) in myeloproliferative disorders results in fusion of the ETS-like TEL gene on 12p13 to the MN1 gene on 22q11., Oncogene. 10 (1995) 1511–1519.

[12] A. Buijs, L. van Rompaey, A.C. Molijn, J.N. Davis, A.C.O. Vertegaal, M.D. Potter, C.

Adams, S. van Baal, E.C. Zwarthoff, M.F. Roussel, G.C. Grosveld, The MN1-TEL Fusion Protein, Encoded by the Translocation (12;22)(p13;q11) in Myeloid Leukemia, Is a Transcription Factor with Transforming Activity, Mol. Cell. Biol. 20 (2000) 9281–9293. https://doi.org/10.1128/mcb.20.24.9281-9293.2000.

[13] M.A. Meester-Smoor, M. Vermeij, M.J.L. van Helmond, A.C. Molijn, K.H.M. van Wely, A.C.P. Hekman, C. Vermey-Keers, P.H.J. Riegman, E.C. Zwarthoff, Targeted Disruption of the Mn1 Oncogene Results in Severe Defects in Development of Membranous Bones of the Cranial Skeleton , Mol. Cell. Biol. 25 (2005) 4229–4236. https://doi.org/10.1128/mcb.25.10.4229-4236.2005.

[14] X. Zhang, D.R. Dowd, M.C. Moore, T.A. Kranenburg, M.A. Meester-Smoor, E.C. Zwarthoff, P.N. MacDonald, Meningioma 1 is required for appropriate osteoblast proliferation, motility, differentiation, and function, J. Biol. Chem. 284 (2009) 18174–18183. https://doi.org/10.1074/jbc.M109.001354.

[15] L.F. Pallares, P. Carbonetto, S. Gopalakrishnan, C.C. Parker, C.L. Ackert-Bicknell, A.A. Palmer, D. Tautz, Mapping of Craniofacial Traits in Outbred Mice Identifies Major Developmental Genes Involved in Shape Determination, PLoS Genet. 11 (2015) 1–25. https://doi.org/10.1371/journal.pgen.1005607.

[16] ensembl, chromosome 5 house mouse Mn1, (2021). https://www.ensembl.org/Mus_musculus/Location/View?db=core;g=ENSMUSG00000070576;r=5:111563401-111604658. (02.04.2022)

[17] H. Kodama, Y. Amagai, H. Sudo, S. Kasai, S. Yamamoto, Establishment of a clonal osteogenic cell line from newborn mouse calvaria, Japanese J. Oral Biol. 23 (1981) 899–901. https://doi.org/10.2330/joralbiosci1965.23.899.

[18] H. Sudo, H.A. Kodama, Y. Amagai, S. Yamamoto, S. Kasai, In vitro differentiation and calcification in a new clonal osteogenic cell line derived from newborn mouse calvaria, J. Cell Biol. 96 (1983) 191–198. https://doi.org/10.1083/jcb.96.1.191.

[19] P.W. Hwang, J.A. Horton, Variable osteogenic performance of MC3T3-E1 subclones impacts their utility as models of osteoblast biology, Sci. Rep. 9 (2019) 1–9. https://doi.org/10.1038/s41598-019-44575-8.

[20] D. Wang, K. Christensen, K. Chawla, G. Xiao, P.H. Krebsbach, R.T. Franceschi, Isolation and characterization of MC3T3-E1 preosteoblast subclones with distinct in vitro and in vivo differentiation/mineralization potential, J. Bone Miner. Res. 14 (1999) 893–903. https://doi.org/10.1359/jbmr.1999.14.6.893.

[21] ATCC, MC3T3-E1 Subclone 4 (ATCC ® CRL-2593 ™), 4 (2015) 2593. https://www.atcc.org/products/crl-2593. (02.04.2022)

[22] Y. Tsuneoka, H. Funato, Modified in situ Hybridization Chain Reaction Using Short Hairpin DNAs, Front. Mol. Neurosci. 13 (2020) 1–14. https://doi.org/10.3389/fnmol.2020.00075.

[23] M. Jinek, K. Chylinski, I. Fonfara, M. Hauer, J.A. Doudna, E. Charpentier, A Programmable Dual-RNA – Guided DNA Endonuclease in Adaptive Bacterial Immunity, 337 (2012) 816–822.

[24] F.A. Ran, P.D. Hsu, J. Wright, V. Agarwala, D.A. Scott, F. Zhang, Genome engineering using the CRISPR-Cas9 system, Nat. Protoc. 8 (2013) 2281–2308. https://doi.org/10.1038/nprot.2013.143. (03.04.2022)

[25] Synthego, Importance of the PAM Sequence in CRISPR Experiments, (2019). https://www.synthego.com/guide/how-to-use-crispr/pam-sequence. (03.04.2022)

[26] Synthego, CRISPR Editing is All About DNA Repair Mechanisms, (2019). https://www.synthego.com/blog/crispr-dna-repair-pathways. (03.04.2022)

[27] F. Zhang, pSpCas9(BB)-2A-GFP (PX458), (n.d.). https://www.addgene.org/48138/.

[28] promega, Transfection, (n.d.). https://www.promega.de/resources/guides/cell-biology/transfection/. (02.04.2022)

[29] Thermo Fisher, Lipofectamine 2000 Transfection Reagent, (n.d.). https://www.thermofisher.com/de/de/home/brands/product-brand/lipofectamine/lipofectamine-2000.html. (03.04.2022)

[30] I. Bio-Rad Laboratories, Flow Cytometry: Cell Analysis vs. Cell Sorting, (2022). https://www.bio-rad.com/featured/en/flow-cytometer.html. (02.04.2022)

[31] E.S. Lander, L.M. Linton, B. Birren, C. Nusbaum, M.C. Zody, J. Baldwin, K. Devon, K. Dewar, M. Doyle, W. FitzHugh, R. Funke, D. Gage, K. Harris, A. Heaford, J. Howland, L. Kann, J. Lehoczky, R. LeVine, P. McEwan, K. McKernan, J. Meldrim, J.P. Mesirov, C. Miranda, W. Morris, J. Naylor, C. Raymond, M. Rosetti, R. Santos, A. Sheridan, C. Sougnez, N. Stange-Thomann, N. Stojanovic, A. Subramanian, D. Wyman, J. Rogers, J. Sulston, R. Ainscough, S. Beck, D. Bentley, J. Burton, C. Clee, N. Carter, A. Coulson, R. Deadman, P. Deloukas, A. Dunham, I. Dunham, R. Durbin, L. French, D. Grafham, S. Gregory, T. Hubbard, S. Humphray, A. Hunt, M. Jones, C. Lloyd, A. McMurray, L. Matthews, S. Mercer, S. Milne, J.C. Mullikin, A. Mungall, R. Plumb, M. Ross, R. Shownkeen, S. Sims, R.H. Waterston, R.K. Wilson, L.W. Hillier, J.D. McPherson, M.A. Marra, E.R. Mardis, L.A. Fulton, A.T. Chinwalla, K.H. Pepin, W.R. Gish, S.L. Chissoe, M.C. Wendl, K.D. Delehaunty, T.L. Miner, A. Delehaunty, J.B. Kramer, L.L. Cook, R.S. Fulton, D.L. Johnson, P.J. Minx, S.W. Clifton, T. Hawkins, E. Branscomb, P. Predki, P. Richardson, S. Wenning, T. Slezak, N. Doggett, J.-F. Cheng, A. Olsen, S. Lucas, C. Elkin, E. Uberbacher, M. Frazier, R.A. Gibbs, D.M. Muzny, S.E. Scherer, J.B. Bouck, E.J. Sodergren, K.C. Worley, C.M. Rives, J.H. Gorrell, M.L. Metzker, S.L. Naylor, R.S. Kucherlapati, D.L. Nelson, G.M. Weinstock, Y. Sakaki, A. Fujiyama, M. Hattori, T. Yada, A. Toyoda, T. Itoh, C. Kawagoe, H. Watanabe, Y. Totoki, T. Taylor, J. Weissenbach, R. Heilig, W. Saurin, F. Artiguenave, P. Brottier, T. Bruls, E. Pelletier, C. Robert, P. Wincker, A. Rosenthal, M. Platzer, G. Nyakatura, S. Taudien, A. Rump, D.R. Smith, L. Doucette-Stamm, M. Rubenfield, K. Weinstock, H.M. Lee, J. Dubois, H. Yang, J. Yu, J. Wang, G. Huang, J. Gu, L. Hood, L. Rowen, A. Madan, S. Qin, R.W. Davis, N.A. Federspiel, A.P. Abola, M.J. Proctor, B.A. Roe, F. Chen, H. Pan, J. Ramser, H. Lehrach, R. Reinhardt, W.R. McCombie, M. de la Bastide, N. Dedhia, H. Blöcker, K. Hornischer, G. Nordsiek, R. Agarwala, L. Aravind, J.A. Bailey, A. Bateman, S. Batzoglou, E. Birney, P. Bork, D.G. Brown, C.B. Burge, L. Cerutti, H.-C. Chen, D. Church, M. Clamp, R.R. Copley, T. Doerks, S.R. Eddy, E.E. Eichler, T.S. Furey, J. Galagan, J.G.R. Gilbert, C. Harmon, Y. Hayashizaki, D. Haussler, H. Hermjakob, K. Hokamp, W. Jang, L.S. Johnson, T.A. Jones, S. Kasif, A. Kaspryzk, S. Kennedy, W.J. Kent, P. Kitts, E. V Koonin, I. Korf, D. Kulp, D.

Lancet, T.M. Lowe, A. McLysaght, T. Mikkelsen, J. V Moran, N. Mulder, V.J. Pollara, C.P. Ponting, G. Schuler, J. Schultz, G. Slater, A.F.A. Smit, E. Stupka, J. Szustakowki, D. Thierry-Mieg, J. Thierry-Mieg, L. Wagner, J. Wallis, R. Wheeler, A. Williams, Y.I. Wolf, K.H. Wolfe, S.-P. Yang, R.-F. Yeh, F. Collins, M.S. Guyer, J. Peterson, A. Felsenfeld, K.A. Wetterstrand, R.M. Myers, J. Schmutz, M. Dickson, J. Grimwood, D.R. Cox, M. V Olson, R. Kaul, C. Raymond, N. Shimizu, K. Kawasaki, S. Minoshima, G.A. Evans, M. Athanasiou, R. Schultz, A. Patrinos, M.J. Morgan, I.H.G.S. Consortium, C. for G.R. Whitehead Institute for Biomedical Research, T.S. Centre:, W.U.G.S. Center, U.S.D.O.E.J.G. Institute:, B.C. of M.H.G.S. Center:, R.G.S. Center:, G. and C. UMR-8030:, I. of M.B. Department of Genome Analysis, G.T.C.S. Center:, B.G.I.G. Center:, T.I. for S.B. Multimegabase Sequencing Center, S.G.T. Center:, U. of O.A.C. for G. Technology:, M.P.I. for M. Genetics:, L.A.H.G.C. Cold Spring Harbor Laboratory, G.R.C. for Biotechnology:, also includes individuals listed under other headings): *Genome Analysis Group (listed in alphabetical order, U.S.N.I. of H. Scientific management: National Human Genome Research Institute, S.H.G. Center:, U. of W.G. Center:, K.U.S. of M. Department of Molecular Biology, U. of T.S.M.C. at Dallas:, U.S.D. of E. Office of Science, T.W. Trust:, Initial sequencing and analysis of the human genome, Nature. 409 (2001) 860–921. https://doi.org/10.1038/35057062.

[32] C. Mülhardt, Der Experimentator: Molekularbiologie/Genomics, 6th ed., Spektrum Akademischer Verlag, 2008.

[33] R. Narayan, Encyclopedia of Biomedical Engineering, 1st ed., Elsevier, 2019.

[34] X.Z. Yan, W. Yang, F. Yang, M. Kersten-Niessen, J.A. Jansen, S.K. Both, Effects of continuous passaging on mineralization of MC3T3-E1 cells with improved osteogenic culture protocol, Tissue Eng. - Part C Methods. 20 (2014) 198–204. https://doi.org/10.1089/ten.tec.2012.0412.

[35] PromoCell GmbH, Osteoblast Differentiation and Mineralization, (2017). https://promocell.com/app/uploads/2017/11/Osteoblast_Differentiation_and_Mineralization-1.pdf. (01.04.2022)

[36] S. Aldrich, Immunodetection Using BCIP/NBT Substate, (n.d.). https://www.sigmaaldrich.com/DE/de/technical-documents/protocol/protein-biology/western-blotting/bcip-nbt-immunodetection. (01.04.2022)

[37] H. Puchtler, S.N. Meloan, M.S. Terry, On the history and mechanism of Alizarin and Alizarin Red S stins for calcium, J. Histochem. Cytochem. (1969).

[38] P.D. Pajevic, Alizarin Red S staining, Massachusetts Generaal Hosp. Harvard Med. Sch. (2017). https://www.csr-mgh.org/wp-content/uploads/2017/04/Alizarin_Red-1.pdf. (02.04.2022)

[39] Top tip bio, Nanodrop results analizing, (n.d.). https://toptipbio.com/the-nanodrop-results-explained/. (02.04.2022)

[40] D. Modrzejewski, F. Hartung, T. Sprink, D. Krause, C. Kohl, R. Wilhelm, What is the available evidence for the range of applications of genome-editing as a new tool for plant trait modification and the potential occurrence of associated off-target effects: a systematic map, Environ. Evid. 8 (2019) 27. https://doi.org/10.1186/s13750-019-0171-5.

[41] abcam, Propidium Iodide, (n.d.). https://www.abcam.com/propidium-iodide-ab14083.html. (04.04.2022)

9. Attachments

9.1 FACS parameter settings

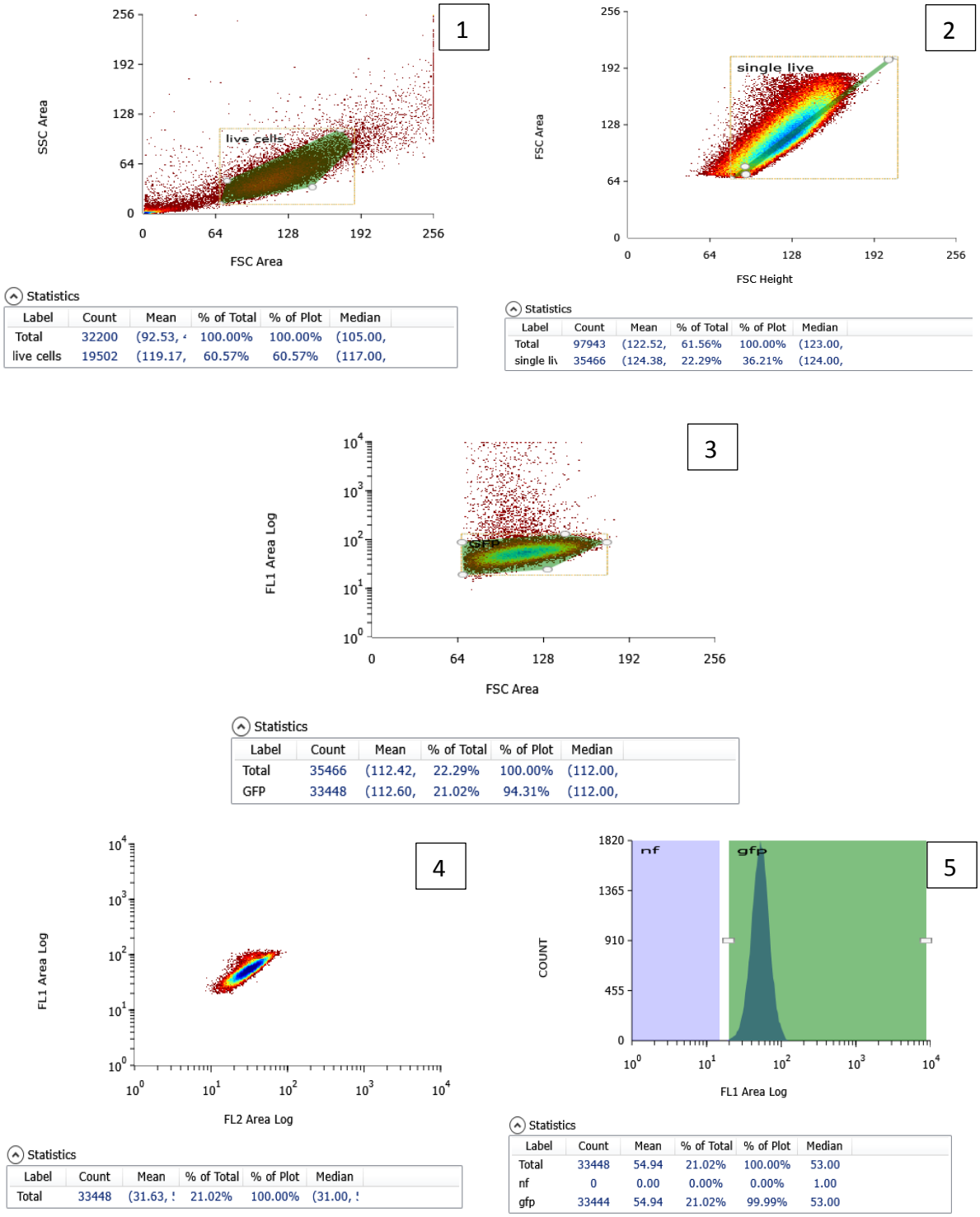

Figure 19: Parameter for FACS sorting of cells transfected with sgRNA1 und sgRNA2

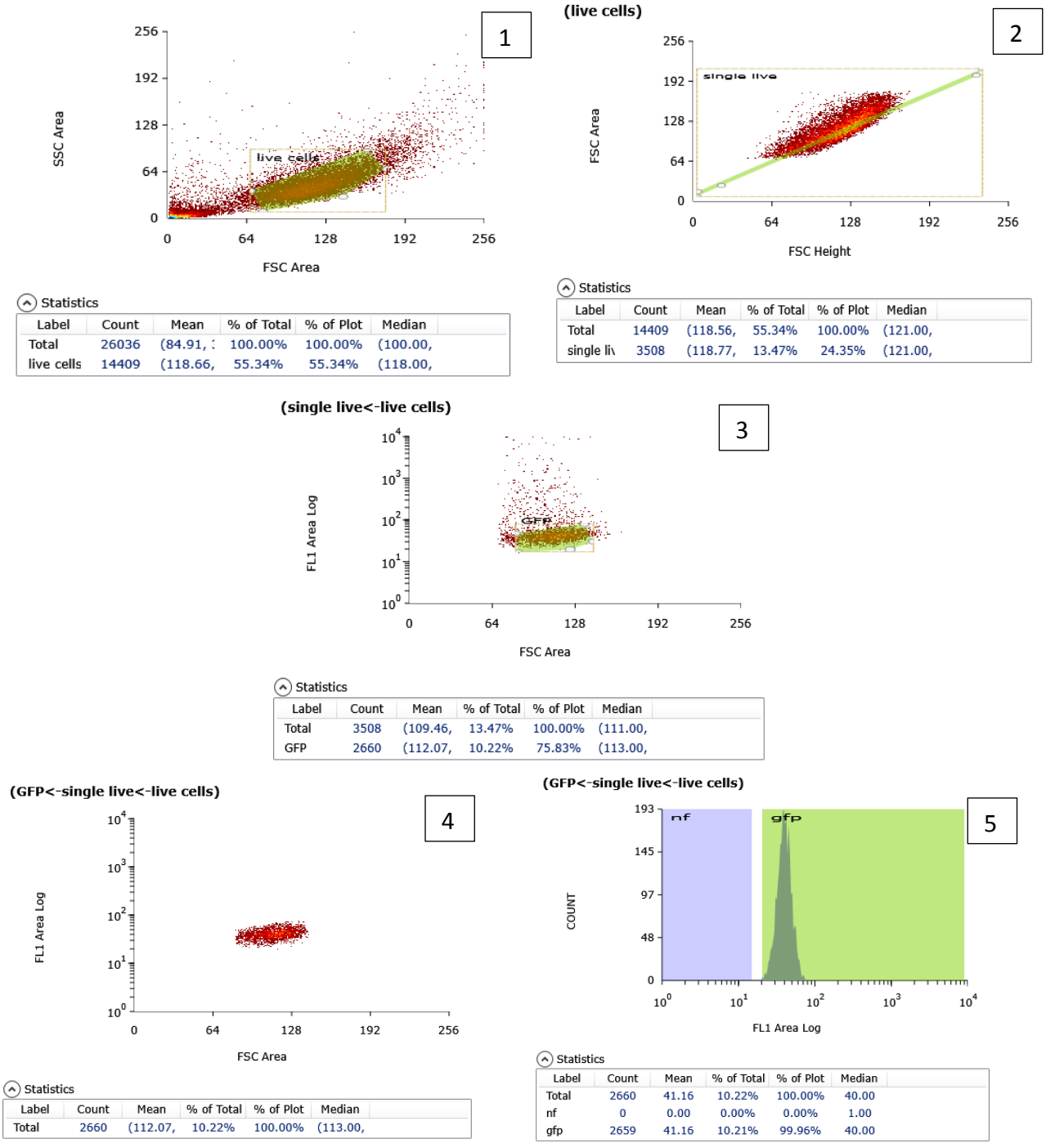

Figure 20: Parameter for FACS sorting of cells transfected with dgRNA

9.2 Optimised FACS parameter settings

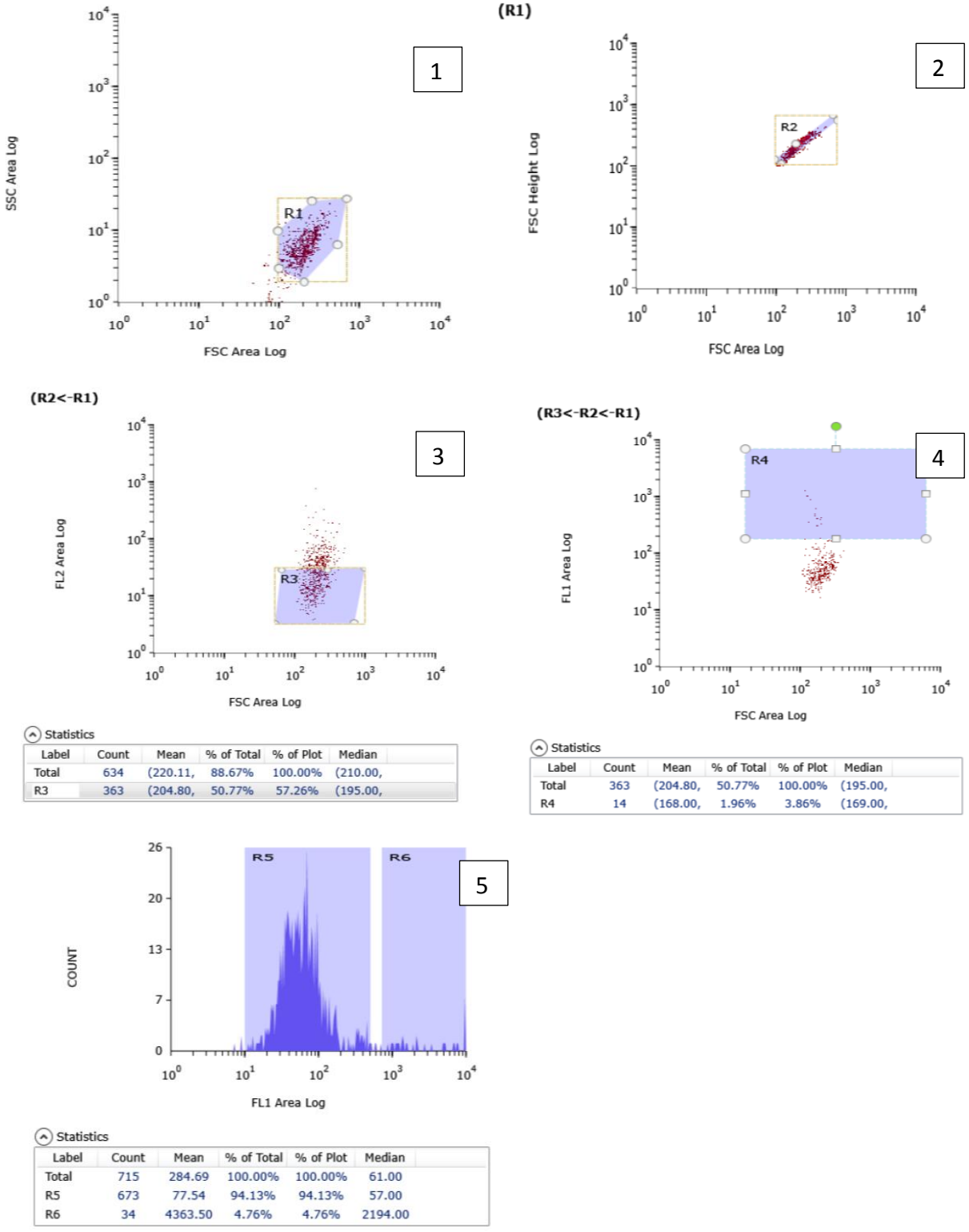

Figure 21: Optimized parameter for FACS sorting of cells transfected with sgRNA1 and sgRNA2

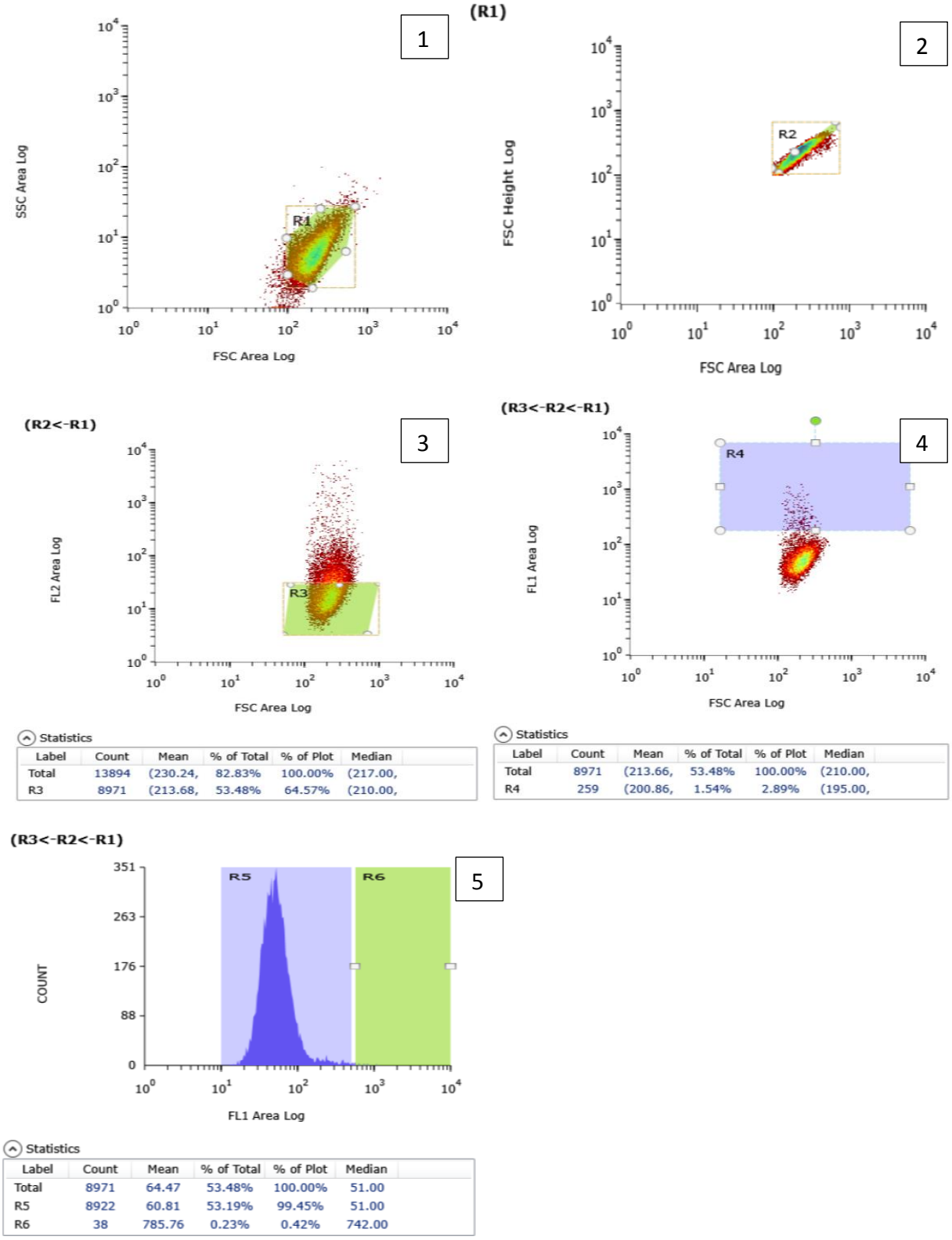

Figure 22: Optimized Parameter for FACS sorting of cells transfected with dgRNA

9.3 Genotyping Nanodrop results

Table 9: Nanodrop results of extracted DNA from clones transfected with plasmid 1

Clone	λ [nm]	A-260 10 mm path	A-280 10 mm path	260/280	260/230	DNA [ng/µl]
1.3	230	1.720	0.823	2.09	2.09	86
1.5	230	2.847	1.376	2.07	2.10	142
1.7	230	1.746	0.835	2.09	1.75	87
1.11	230	0.367	0.179	2.05	1.32	18
1.12	230	1.209	0.622	1.94	1.43	61
1.15	230	2.372	1.245	1.90	1.19	119
1.16	230	0.955	0.552	1.73	1.12	48
1.18	230	0.931	0.397	2.35	1.44	47
1.21	230	0.355	0.203	1.75	0.87	18
1.22	230	0.595	0.324	1.84	1.21	30
1.24	230	1.136	0.683	1.66	0.75	57
1.25	230	0.639	0.327	1.96	1.32	32
1.27	230	0.832	0.430	1.93	1.43	42
1.28	230	2.241	1.122	2.00	2.01	112
1.31	230	0.803	0.366	2.19	1.82	40
1.33	230	0.643	0.373	1.72	1.01	32
1.35	230	0.617	0.314	1.97	1.19	31
1.37	230	1.865	1.199	1.56	0.63	93
1.38	230	0.513	0.275	1.87	0.75	26
1.40	230	0.580	0.325	1.78	0.83	29
1.41	230	0.578	0.348	1.66	1.05	29
1.42	230	0.691	0.354	1.95	1.22	35
1.44	230	0.429	0.252	1.70	0.72	21
1.46	230	0.548	0.257	2.13	1.44	27

Table 10: Nanodrop results of extracted DNA from clones transfected with plasmid 2

Clone	λ [nm]	A-260 10 mm path	A-280 10 mm path	260/280	260/230	DNA [ng/µl]
2.1	230	2.242	1.180	1.90	1.71	112
2.2	230	3.411	1.775	1.92	1.68	171
2.3	230	1.245	0.706	1.76	1.32	62
2.4	230	1.337	0.684	1.96	1.15	67
2.5	230	1.316	0.682	1.93	1.07	66
2.6	230	1.061	0.584	1.82	1.18	53
2.7	230	1.252	0.674	1.86	1.40	63
2.8	230	0.941	0.474	1.98	1.17	47
2.11	230	0.380	0.202	1.89	0.73	19
2.14	230	0.836	0.457	1.83	1.06	42
2.17	230	0.275	0.188	1.46	0.60	14
2.20	230	0.732	0.467	1.57	0.77	37
2.22	230	0.545	0.318	1.71	0.85	27
2.24	230	0.891	0.483	1.85	1.29	45
2.27	230	0.282	0.187	1.51	0.56	14
2.31	230	0.921	0.460	2.00	1.66	46
2.56	230	0.501	0.249	2.01	0.79	25
2.58	230	1.060	0.556	1.91	1.24	53
2.61	230	1.307	0.860	1.52	0.69	65
2.64	230	0.615	0.384	1.60	0.94	31
2.66	230	0.237	0.148	1.61	0.67	12
2.68	230	0.416	0.167	2.48	1.06	21
2.70	230	0.518	0.301	1.72	0.94	26
2.72	230	0.400	0.241	1.66	0.94	20

Table 11: Nanodrop results of extracted DNA from clones transfected with plasmid dgRNA

Clone	λ [nm]	A-260 10 mm path	A-280 10 mm path	260/280	260/230	DNA [ng/ µl]
4.1	230	0.788	0.391	2.02	1.01	39
4.2	230	0.326	0.182	1.79	0.62	16
4.3	230	0.888	0.392	2.27	1.92	44
4.4	230	0.811	0.375	2.16	1.08	41
4.5	230	0.653	0.275	2.37	1.27	33
4.6	230	0.795	0.380	2.09	1.31	40
4.7	230	2.462	1.201	2.05	1.77	123
4.8	230	0.782	0.422	1.85	1.11	39
4.9	230	0.721	0.354	2.04	1.41	36
4.10	230	0.920	0.441	2.08	1.24	46
4.11	230	0.640	0.321	1.99	1.08	32
4.12	230	0.825	0.412	2.00	0.99	41
4.13	230	0.858	0.489	1.75	1.10	43
4.14	230	0.473	0.308	1.53	0.82	24
4.15	230	0.943	0.504	1.87	1.67	47
4.16	230	0.183	0.116	1.57	0.45	9
4.17	230	1.084	0.542	2.00	1.66	54
4.18	230	0.691	0.354	1.95	1.22	35
4.19	230	0.749	0.432	1.73	0.82	37
4.20	230	0.517	0.282	1.83	0.80	26
4.21	230	0.591	0.320	1.85	0.95	30
4.22	230	0.430	0.248	1.73	0.76	21
4.23	230	0.998	0.552	1.82	1.09	50
4.24	230	0.907	0.478	1.90	1.23	45

9.4 ARS plate reader measurements and calculations

Table 12: standard curve raw data

	Ext. [-]	mean (*M*)
1.1	1.456599951	
1.2	1.4648	1.460699975
2.1	1.129500031	
2.2	1.105000019	1.117250025
3.1	0.408699989	
3.2	0.414799988	0.411749989
4.1	0.1373	
4.2	0.1373	0.1373
5.1	0.090400003	
5.2	0.089100003	0.089750003
6.1	0.064300001	
6.2	0.065399997	0.064849999
7.1	0.042399999	
7.2	0.042300001	0.04235

Table 13: calculations for Mol concentrations of ARS-bound calcium after extracting with 10% CPC of MC3T3-E1 Passage 9

Ext. Blank (10% CPC): 0.0424						
	D7 Ext. [-]	**mean (*M*)**	***M* - Blank**	**in mol ARS**	***M* mol ARS**	**standard deviation**
1.1 1.2	0.3348 0.3211	0.32795	0.28555	0.00936604	0.00944312	5.4606E-05
2.1 2.2	0.33669999 0.3265	0.3316	0.2892	0.00948576		
3.1 3.2	0.3362 0.3265	0.33135	0.28895	0.00947756		
	D10 Ext. [-]	**mean (*M*)**	***M* - Blank**	**in mol ARS**	***M* mol ARS**	**standard deviation**
1.1 1.2	0.477 0.46849999	0.47274999	0.43034999	0.01411548	0.01417725	8.969E-05
2.1 2.2	0.46259999 0.48269999	0.47264999	0.43024999	0.0141122		
3.1 3.2	0.4702 0.48679999	0.47849999	0.43609999	0.01430408		
	D14 Ext. [-]	**mean (*M*)**	***M* - Blank**	**in mol ARS**	***M* mol ARS**	**standard deviation**
1.1 1.2	0.43130001 0.46900001	0.45015001	0.40775001	0.0133742	0.01271055	0.00048692
2.1 2.2	0.41049999 0.43880001	0.42465	0.38225	0.0125378		
3.1 3.2	0.40130001 0.42860001	0.41495001	0.37255001	0.01221964		
	ctrl Ext. [-]	**mean (*M*)**	***M* - Blank**	**in mol ARS**	***M* mol ARS**	**standard deviation**
1.1 1.2	0.28999999 0.27160001	0.2808	0.2384	0.00781952	0.00904296	0.00088604
2.1 2.2	0.33219999 0.32699999	0.32959999	0.28719999	0.00942016		
3.1 3.2	0.34369999 0.3441	0.3439	0.3015	0.0098892		
						M: 0.00037931

Table 14: calculations for Mol concentrations of ARS-bound calcium after extracting with 10% CPC MC3T3-E1 Passage 6

	D14 Ext. [-]	**mean (*M*)**	***M* - Blank**	**in mol ARS**	***M* mol ARS**	**standard deviation**
1.1 1.2	0.50989997 0.56510001	0.53749999	0.4951	0.01623928	0.01556305	0.00048094
2.1 2.2	0.49649999 0.5205	0.50849999	0.4661	0.01528808		
3.1 3.2	0.49810001 0.51120001	0.50465001	0.46225001	0.0151618		
	D21 Ext. [-]	**mean (*M*)**	***M* - Blank**	**in mol ARS**	***M* mol ARS**	**standard deviation**
1.1 1.2	1.39649999 1.46089995	1.42869997	1.38629997	0.04547064	0.04075673	0.0080346
2.1 2.2	0.92470002 0.95560002	0.94015002	0.89775002	0.0294462		
3.1 3.2	1.45480001 1.51740003	1.48610002	1.44370002	0.04735336		
	ctrl Ext. [-]	**mean (*M*)**	***M* - Blank**	**in mol ARS**	***M* mol ARS**	**standard deviation**

1.1 1.2	0.33930001 0.33840001	0.33885001	0.29645001	0.00972356	0.01115747	0.00104585
2.1 2.2	0.39930001 0.39039999	0.39485	0.35245	0.01156036		
3.1 3.2	0.41370001 0.41429999	0.414	0.37160001	0.01218848		
						M: 0.00318713

9.4 Triplicates of the stainings

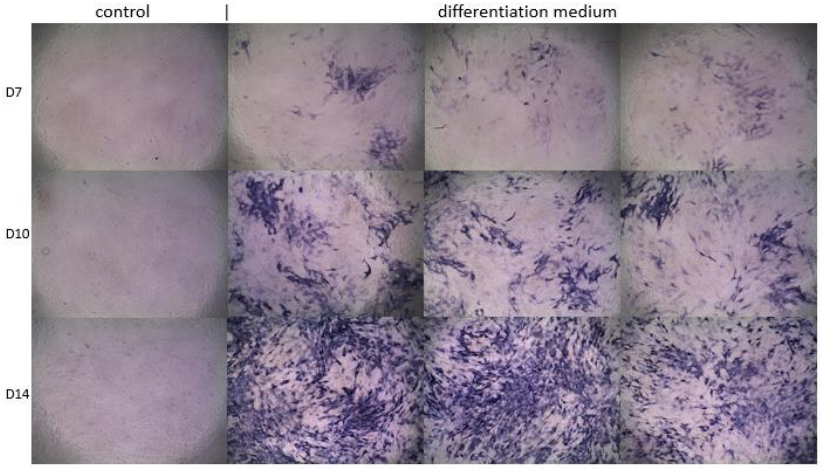

Figure 23: BCIP/NBT staining for alkaline phosphatase in MC3T3-E1 passage 9

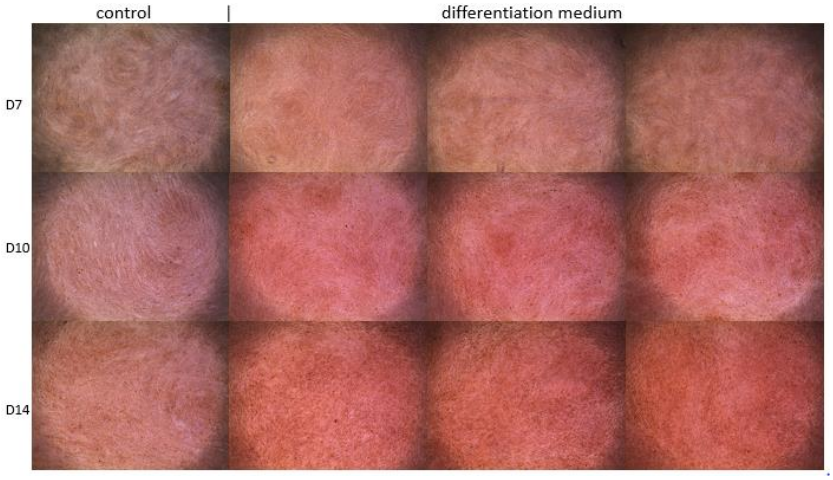

Figure 24: Alizarin Red S staining for Calcium in MC3T3-E1 passage 9

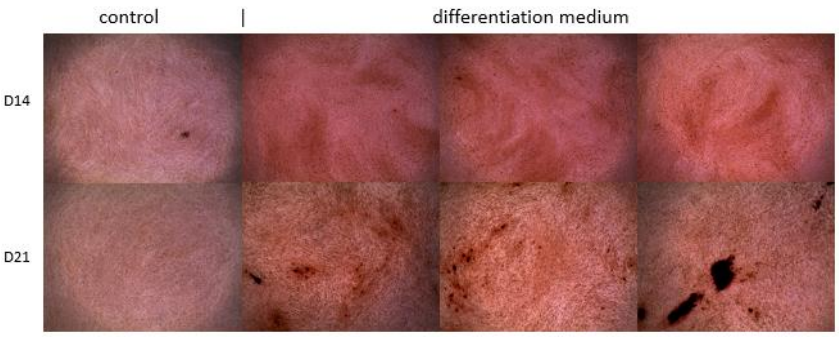

Figure 25: Alizarin Red S staining for Calcium in MC3T3-E1 passage 6

10. Author’s declaration

Ich versichere, dass ich die vorliegende Thesis ohne fremde Hilfe selbstständig verfasst und nur die angegebenen Quellen benutzt habe.

Flensburg den 7. April 2022

_____

Wiebensohn, Clara